Journal of Engineering and Computer Sciences
Vol. 17, No. 02, pp. 21-54 (July-Dec 2025)

Assessing the Impact of Electric Vehicle and Renewable Energy Integration on Distribution System Performance

Bandar Alrashidi
Department of Electrical Engineering, College of Engineering, Qassim University, Buraidah 52571, Saudi Arabia.
E: 461115479@qu.edu.sa

Abdulrahman Alsafrani
Department of Electrical Engineering, College of Engineering, Qassim University, Buraidah 52571, Saudi Arabia.
E: a.alsafrani@qu.edu.sa

Ahmad Eid, Senior Member, IEEE
Department of Electrical Engineering, College of Engineering, Qassim University, Buraidah 52571, Saudi Arabia.
E: a.mohamad@qu.edu.sa

[Received: 14 November 2025, Revised: 01 January 2026, Accepted: 19 January 2026, Published Feb 2026]

Abstract: A rapid increase in electric-vehicle (EV) adoption is imposing new stresses on distribution feeders, yet quantitative evidence on how coordinated renewable generation and vehicle-to-grid (V2G) operation can mitigate these impacts remains limited, especially for radial networks with long laterals and evening-peaking demand. In this study, high-resolution (15-min) time-series power-flow simulations were performed on canonical 69-bus radial system to evaluate uncontrolled EV charging, managed charging with V2G triggers, and combined scenarios with feeder-embedded photovoltaics (PV) and wind turbine generation (WTG). A stochastic EV arrival model, battery state-of-charge tracking, and a simple charger model (2.3 kW per phase, pf≈0.95) were adopted; V2G discharging was activated when local voltage fell below 0.95 pu (V_on) and deactivated when voltage recovered above 0.97 pu (V_off) or when SoC reached the lower bound, to avoid chattering. PV/WTG outputs followed realistic diurnal profiles with lagging power factors representative of inverter limits. Backward/forward-sweep load flow yielded node voltages, branch currents, and total feeder losses across a 24-h horizon, and results were synthesized via heat maps, box plots, and daily power balance curves. It was found that coordinated V2G with feeder-level PV/WTG materially reduces peak source current, alleviates trunk and mid-feeder overloading, and lowers total active power losses, while lifting minimum voltages toward acceptable limits during critical evening windows. Benefits were strongest when renewable production temporally overlapped charging demand and where DERs were electrically proximate to stressed branches; residual constraints persisted during late-night peaks with weak renewable support. Overall, the results indicate that pragmatic V2G thresholds, modest feeder-sited renewables, and basic charging management can substantially improve hosting capacity without immediate network reinforcement.

Keywords*:* Electric vehicles; Distribution networks; Vehicle-to-Grid (V2G); Photovoltaics; Wind generation; Power loss reduction; Voltage regulation.

1. INTRODUCTION

Electric power systems are undergoing a structural transition as transportation electrifies at scale. Electric vehicles (EVs) reshape not only the magnitude of electricity demand but also its temporal and spatial patterns, creating new stress points on distribution feeders and assets. A broad body of evidence shows that unmanaged charging can cluster in evening peaks, driving feeder congestion, accelerating thermal aging of transformers and cables, and provoking voltage excursions especially in networks already hosting large amounts of inverter-based generation [1]–[3]. In parallel, public and private charging infrastructure is expanding quickly, which is necessary for adoption yet amplifies planning and operational

complexity for distribution system operators (DSOs) [2], [4]. These shifts motivate integrated energy-transport planning frameworks that co-optimize siting, sizing, and operational policies for EV supply equipment (EVSE) and distributed energy resources (DERs).

A complementary strand focuses on coordinated (managed) charging, with and without vehicle-to-grid (V2G). Coordinated charging shifts EV demand away from stressed periods and aligns it with renewable availability and network headroom; numerous studies report substantial reductions in congestion and voltage violations when even simple scheduling is deployed [4]. More advanced formulations incorporate feeder constraints into charging optimization or jointly plan EVSE locations and sizes alongside network reinforcements [11], [14], [15]. The V2G proposition leveraging EV batteries for peak shaving, voltage support, and ancillary services remains technically compelling but practically nuanced, with net benefits contingent on battery aging costs, user acceptance, and aggregator design [16]. Early pilots and model-based analyses suggest that V2G adds incremental value under specific duty cycles and compensation structures, but managed charging often delivers the largest impact-per-cost when first deployed at scale [4], [16].

The primary aim of this work is to develop and evaluate an integrated framework that minimizes EV-driven feeder impacts losses, congestion, and voltage non-compliance by combining:

1. Spatial planning of renewable DERs (PV/wind) through sensitivity-informed and optimization-based siting/sizing aligned with EV demand patterns.
2. Operational controls that employ grid-supportive inverter functions and managed charging (with optional V2G where net benefits exceed aging penalties).
3. Time-series distribution-flow simulation with uncertainty-aware inputs that reflect empirically grounded charging behaviour and renewable variability.

By cross-comparing portfolios across realistic adoption and resource scenarios, the study is designed to isolate the marginal value of each lever and their synergies under standards-consistent operating envelopes and power-quality constraints. We anticipate concluding that: (i) co-designed DER siting and inverter controls can raise EV hosting capacity significantly above baseline; (ii) managed charging delivers high impact-per-cost when aligned with DER availability and feeder topology; (iii) V2G provides incremental benefits under targeted duty cycles and compensation regimes but is not universally superior once battery aging and user utility are internalized; and (iv) rigorous attention to transformer/cable thermal limits and harmonic interactions is indispensable to avoid asset over-stress and power-quality regressions during clustered charging events [3], [4], [6], [11], [12], [15], [16].

Contributions of this paper are:

- 15-min time-series assessment of EV charging with optional V2G on the IEEE 69-bus feeder.
- Integrated comparison of EV-only, PV+EV/V2G, and PV+WTG+EV/V2G portfolios using consistent KPIs (Vmin, Isrc, TPL).
- Explicit, reproducible control logic for V2G triggering (with hysteresis) and SoC bounds.
- Sensitivity-informed DG siting using an LSF.

2. SYSTEM MODELING AND METHODOLOGY

This study adopts a focused, distribution-level modeling scope that is consistent with the implemented MATLAB code and the IEEE-69 feeder benchmark. The objective is to isolate the dominant steady-state interactions among bus-level EV charging/V2G and fixed-power-factor DER (PV and wind) under radial operation, using a transparent per-unit formulation and a Backward/Forward Sweep (BFS) power-flow solver [17]–[20].

Modeling assumptions

- Network topology and phase model. The system is a radial feeder instantiated as IEEE-69; analysis is performed in a single-phase per-unit representation (phase-to-neutral base), which captures voltage-drop and current-flow effects along the radial paths. Three-phase unbalance, phase coupling, and mutual impedances are not modeled [21]–[25].
- Loads. Bus demands are modeled as constant complex powers ($P + jQ$) per time step.
- EV/V2G behavior. EV sessions follow a bus-local queue with a maximum number of EVs depending on many constrains and simultaneous EVs per bus. Each connected EV charges at specific rated power; SoC evolves in 15-min quanta within declared bounds. A local V2G trigger activates discharging at a bus when the prior-step voltage < 0.95 p.u., with a bounded 70%→50% SoC discharge envelope before resuming charge. Arrival percentages are time-varying and exogenous; random seeds are fixed for reproducibility.
- Power-flow solution. Each 15-min step is solved via BFS to a tight voltage-change tolerance. The slack source is fixed at the per-unit base voltage (angle 0 unless otherwise noted). Discrete equipment controls (OLTC, switched capacitors), protection devices, and fault behavior are not modeled in the base case [26]–[30].
- Time horizon and resolution. Simulations use Δt = 15 min over ≈24 h, sufficient to capture late-afternoon/evening charging and overnight evolution.

These assumptions bound the problem to a transparent, steady-state, time-series screening framework that is reproducible and directly traceable to the implemented solver and input profiles [24].

Topology and bases. The distribution network is radial with a slack bus at the substation (*bus 1*). Calculations use a phase-to-neutral per-unit base defined by $V_{(\text{base})} = V_{ll}/\sqrt{3}$ and declared power base $S_{(\text{base})}$. Branch series impedances $Z_{mn} = R_{mn} + jX_{mn}$ are time-invariant; loads are modeled as constant complex powers at each step. The solver is an explicitly coded BFS suitable for high-R/X radial feeders [25].

DER representation. Distributed sources are modeled as PQ injections with fixed power factor at their assigned buses and time-varying active-power profiles (15-min). Reactive power is inferred via $|Q|/P = \tan \varphi$.

Compliance context. Voltage service bands and thermal limits are checked against the screening criteria referenced previously (ANSI C84.1/EN 50160 for voltage, IEC 60287 for ampacity); harmonic checks per IEEE 519-2022 are optional post-processing indicators when required [29],[30].

The study area comprises standardized benchmark feeders to ensure transparency and reproducibility. The primary system used for method development and scenario analysis is the IEEE-69 bus feeder is listed for optional cross-validation and sensitivity checks.

- Scope. The IEEE-69 feeder as shown in Fig. 1 (radial, higher depth and loading diversity) is identified as an optional benchmark for cross-validation and sensitivity extensions (e.g., different spatial clustering, alternative DER siting) [29].
- Configuration. Unless otherwise stated, the same modeling assumptions apply (single-phase p.u., constant-power loads, fixed-pf PQ DER, EV/V2G rules) with feeder-specific impedances and load data from the benchmark sources.

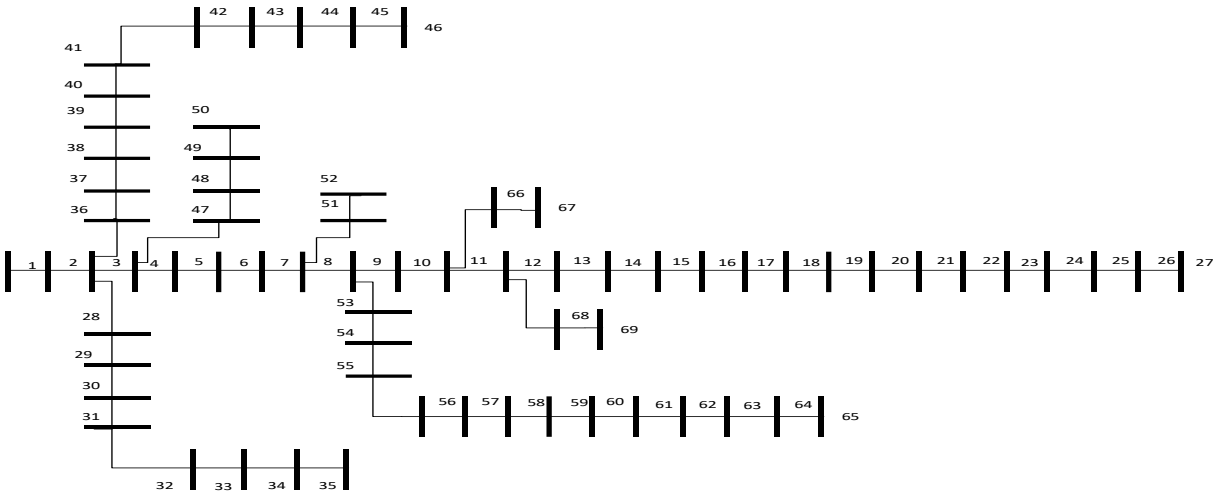

Fig. 1: 69 Bus System Diagram.

2.1. Electric Vehicle Charging, V2G Control, and Power-Flow Formulation

This section formalizes the EV demand model used in the time-series studies. The representation is deliberately modular separating (i) charger nameplate power and power factor, (ii) arrival and parking/dwell processes, and (iii) State-of-Charge (SoC) evolution and queue logic, so it can support baseline and mitigation scenarios without changing core equations.

EV charging spans a wide range of AC and DC power levels depending on the supply voltage, current capability, and equipment class. In residential contexts, a very common baseline is "socket" (Mode 2/low-AC) charging via a standard 230 V household outlet limited to ~10 A, yielding a charging power of about 2.3 kW. Peer-reviewed literature classifies this as low AC (< 2.3 kW) and documents its widespread use for overnight home charging in 230 V regions.

Modern chargers employ active PFC. Base simulations use pf = 0.99 for AC and unity for DC at nominal load. Sensitivity runs consider pf = 0.95 and elevated distortion to reflect degraded PFC or part-load operation. PQ checks reference IEEE 519-2022 limits for current distortion (TDD) and voltage THD at the PCC [25].

Each connection is modeled as an EV session with five attributes: arrival time, dwell (parking) duration, initial state of charge (SoC_0), user target SoC, and a charger nameplate limit. Sessions are admitted through a bus-local queue with a finite number of plugs per bus; when a port is free, the next waiting EV charges at its setpoint. This modular setup supports unmanaged operation as well as managed charging/V2G policies without altering the feeder equations.

In distribution-system studies, the dominant residential pattern is overnight, long-dwell charging at home. Planning studies and industry-wide analyses consistently emphasize that charging at locations with long dwells—at/near home and work—underpins the ecosystem; long-dwell windows are commonly on the order of 8 hours or more, particularly overnight. In our baseline, we therefore treat a typical home session as ≈8 h of available plug-in time. The energy actually added in such a session depends on charger power and efficiencies; for example, a 2.3 kW socket (Mode-2, 230 V×10 A) adds on the order of ~18–20 kWh over 8 h after accounting for charger/battery losses often sufficient to cover a day's driving whereas higher-power wall boxes add proportionally more.

With finite plugs per bus, arriving sessions that find all ports occupied wait in a first-come-first-served queue. Sessions may be pre-empted or rate-limited by control logic (e.g., managed charging to respect transformer limits or V2G discharge bands), but the underlying bookkeeping arrival, admission, SoC update per time step remains unchanged.

As a rule of thumb for home charging, going from a low SoC to the target SoC (e.g., ~90–95%) with a typical 2.3 kW socket charger takes about 8 hours overnight. The actual duration is not fixed: it shortens if the starting SoC is higher (or

the target is lower), and lengthens if starting from very low SoC or using a smaller effective charging power. More generally,

$$t \approx ((\mathrm{SoC} - \mathrm{SoC0}) * \mathrm{E\_max})/(Pcharger * \eta)$$

So charging time varies with the SoC window, battery capacity E_{max} , charger power $P_{charger}$.

State of Charge (SoC)

Building on the session model and the power/power-factor assumptions, the SoC state tracks how much energy an EV battery has at each time step and governs when a session finishes charging (or how far it may discharge under V2G).

SoC is expressed in percent [0,100] % and with health and policy bounds,

$$SoCmin \leq SoCk \leq SoCmax$$

Operating bounds (health-conscious). constrain of SoC to be 20%–95%. The lower bound avoids deep-discharge stress; the upper bound avoids prolonged high-SoC storage, which multiple studies identify as a key driver of calendar aging.

Arrival initialization. In the absence of site-specific telemetry, arrival SoC is drawn randomly within [20%, 95%], ensuring coverage of realistic arrivals from low to high without violating the health-oriented bounds above. This initialization is scenario-configurable.

In distribution-level studies focused on home charging, EV arrivals are typically evening-peaked: most sessions start after the commute and roll into the night, producing a pronounced rise in connections between early evening and late evening with long overnight dwells.

In this work study, home arrivals are represented by an evening-peaked time-of-day distribution at 15-minute resolution (CDF). This curve determines when sessions begin; the resulting energy draw then follows from the session model. The shape (timing) and intensity (penetration) remain scenario-configurable.

The cumulative distribution function F(t) gives the probability that a home-charging session starts at or before time t within a day. Using a CDF lets us generate realistic as shown in Figs. 2 and 3 (evening-peaked) arrival times while keeping the model simple and reproducible, see Fig. 4 for electrical vehicle main data.

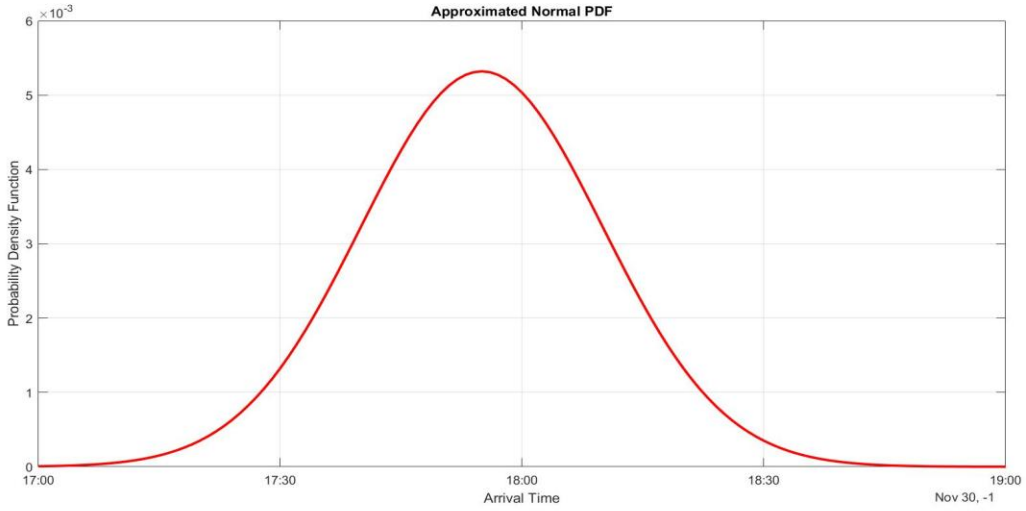

Fig. 2: Nominal PDF.

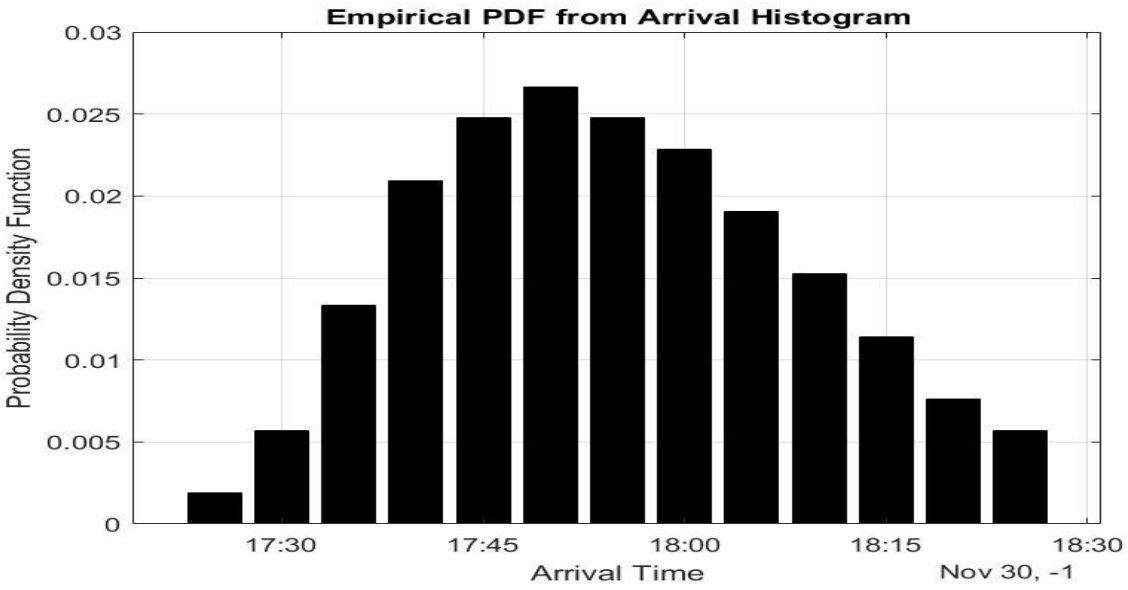

Fig. 3: Empirical PDF.

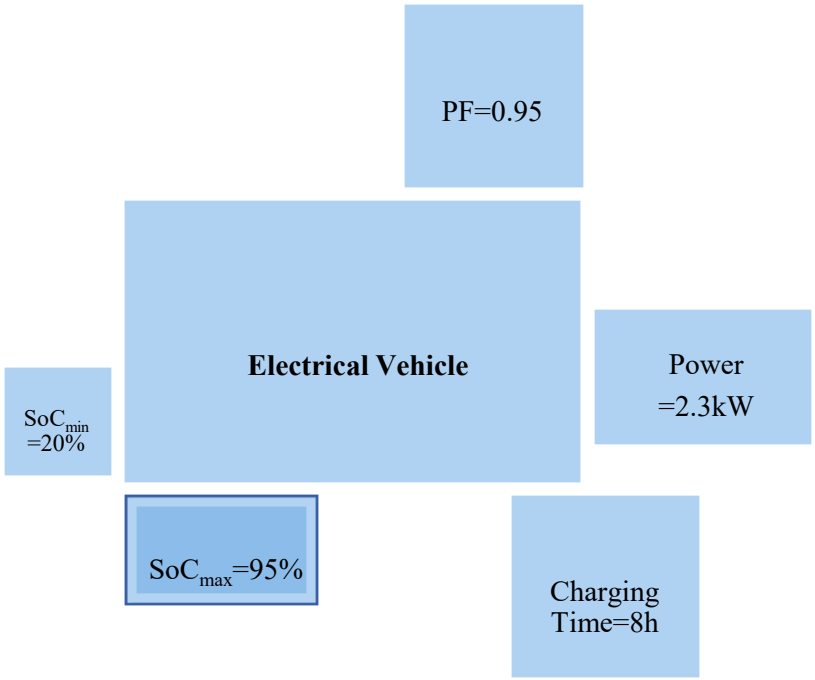

Fig. 4: EV parameters used in the simulations (charger power, power factor, battery energy, efficiencies, and SoC bounds).

In distribution system engineering, the feeder at each time step is represented by nodal complex powers (P + jQ) and line impedances (R + jX) in a per-unit model. EV charging and DER injections are mapped to time-series net injections at each bus, and network performance is evaluated using voltage limits (e.g., 0.95–1.05 pu), branch-current limits, and total I^2R losses.

Load flow analysis plays a critical role in addressing operational and planning challenges in power systems. By considering a defined generation scenario and the configuration of the transmission network, load flow analysis determines the steady-state operating conditions, including node voltages and power flows through branches. It provides insights into the balanced steady-state behavior of the system, focusing on normal operation without accounting for transient dynamics [28], [31].

The Backward/Forward Sweep Method (BFSM) consists of two iterative steps: the forward sweep and the backward sweep. During these steps, current values are calculated, and voltages at each node are updated accordingly. This method does not rely on sequential numbering of branches. Instead, it utilizes a node-branch identification scheme to determine the number of connected branches and nodes beyond a given branch. Using this scheme, all possible paths for power and current flow are systematically computed [17–19].

Initialization

substation (slack bus) voltage:

$$V_{sub}^{(0)} \approx 1.0 \text{ p.u.}$$

All other node voltages: Initialize them to an approximate value

$$V_{sub}^{(0)} \approx 1.0 \text{ p.u.}$$

Backward Sweep:

Starting from the leaf nodes (the most downstream nodes) and moving backward toward the substation, compute branch currents. One common formulation is:

$$I_i^{n+1} = \frac{((P_i - jQ_i)^*)}{\left((V_i^n)^*\right)} + sum_{k \in child(i)} I_k^{n+1} \qquad (1)$$

Forward Sweep:

After obtaining currents Ii(n+1) from the Backward Sweep, move forward from the substation (root node) to the leaf nodes to update voltages. A common formula is:

$$V_j^{n+1} = V_i^{n+1} - Z_{ij} * I_j^{n+1} \qquad (2)$$

EV power aggregation converts behavioral/operational inputs arrival profile, charging-session duration, charger setpoint and power factor into a time series of power at resolution Δt (e.g., 15 min), then combines it with the network's base load. Then Served sessions are mapped to active power assuming a quasi-constant charger setpoint at bus b,

$$Q_{EV(t)} = P_{EV(t)} \tan(\arccos(pf)) \qquad (3)$$

$$S_{EV(t)} = \sqrt{P_{EV(t)}^2 * Q_{EV(t)}^2} \qquad (4)$$

from which conductor currents follow. Copper losses at a line section with resistance R are,

$$P_{loss(t)} = 3 * I_{(t)}^2 * R \qquad (5)$$

Daily energy is obtained by time aggregation:

$$P_{Total(t)} = \sum_{t=0}^{24} P_{(t)} \qquad (6)$$

With these laws, EV aggregation yields consistent spatial temporal power profiles that examine peak demand P_{max}, voltage compliance, thermal loading, and losses.

2.2. Distributed Generation Modeling (PV/WTG) and DG Siting

Distributed generation often framed under "distributed energy resources (DERs)" covers small to medium units located near loads (e.g., rooftop and community PV, small wind, CHP, fuel cells, engine-gensets). Properly integrated, DG can lower losses by serving local demand, defer some grid upgrades, improve resilience, and support decarbonization while also introducing new operational and coordination challenges.

Modern interconnection practice is shaped by IEEE Std 1547-2018, which requires DERs to have voltage/power control capabilities (e.g., Volt-VAR, Volt-Watt), low/high voltage and frequency ride-through, and defined performance at the point of common coupling. These functions turn DG from a "passive" source into an active participant in voltage and frequency support on distribution feeders.

Because legacy feeders were designed for one-way power flow, significant DG penetration can drive voltage rise, reverse power flow, and protection coordination issues (fault level changes, directional sensing, islanding concerns). Industry guidance highlights protection adaptations for LV/MV networks under growing DER levels, both in grid-connected and islanded modes.

Utilities increasingly use hosting capacity the maximum incremental DG that can be connected without breaching limits (voltage, thermal, protection, power quality) to quantify where and how much DG a feeder can accept.

For siting/sizing DG, planners combine fast sensitivity indices (e.g., loss-sensitivity–based bus screening) with optimization to minimize losses, improve voltages, or relieve constraints under network limits. Recent work blends analytical loss-sensitivity with metaheuristics to select buses and ratings efficiently.

When DG follows modern interconnection rules and is placed/sized with feeder limits in mind, it can reduce I^2R losses, bolster voltage profiles, and enhance reliability. As EV charging and other new loads grow, DG's local support (active/reactive power) and strategic siting become even more valuable within standard distribution-planning workflows.

The goal of siting distributed generation (DG) is to maximize benefit (loss reduction, voltage support, reliability) while respecting network limits (voltage bounds, thermal ratings, protection/short-circuit constraints). In practice, buses that are heavily loaded or electrically far from the source often yield larger I2R loss reductions and better local voltage when DG injects power near the demand, but you must check for over-voltage and reverse power flow side effects.

A practical workflow is: (1) screen candidate buses with fast sensitivity indices e.g, Loss Sensitivity Factor (LSF) for active-power placement and a voltage-weakness/stability index for reactive-power support; (2) validate by power flow each shortlisted bus over a reasonable DG size range to confirm voltage compliance, line/transformer loading, protection coordination, and hosting capacity; (3) choose the bus (and size) from the resulting benefit-versus-size curves. When DG can provide reactive power (Volt/Var), prioritizing voltage-weak buses is often advantageous. With multiple DGs, use a simple multi-objective optimization (losses, voltage profile, cost) and ensure phase balance if single-phase units are involved.

Candidate buses for DG siting are ranked by Loss Sensitivity Factors (LSF), the sensitivity of total feeder losses to incremental injection at a bus. With linearized distribution factors around a solved base flow, LSF yields a ranked list of locations with highest marginal loss reduction and is effective as a pre-screen before metaheuristics or multi-objective optimization [28]–[31].

$$LSF = 2 \sum_{\{k=1\}}^{N} R_{ik} * \frac{P_k}{V_k^2} \qquad (7)$$

Single-DG algorithm

- Solve base case; compute losses and voltages.
- Compute LSFs for all buses; select top-k candidates.
- Size each candidate within local hosting-capacity margins.
- Validate by full time-series run; iterate if needed.

Use a constraint-driven approach for multiple DGs: first define the acceptable operating envelope, bus voltages must always stay within the utility's limits, line and transformer currents must remain below ampacity, and feeder losses should be capped or, preferably, minimized. Screen candidate buses, then run time-series power-flow across stress scenarios (low-load/high-DG, high-load/low-DG, and relevant contingencies). Add or co-optimize DGs while continuously checking those three constraints; if any node or line violates a limit, resize, relocate, or retune (e.g., enable Volt/Var or

adjust setpoints) until it's feasible. Prefer spreading several modest units near load pockets to reduce upstream currents and losses, watch phase balance for single-phase DGs [30], [31].

In distribution studies, constraints define the feasible operating envelope over time. Core voltage constraints require every bus to remain within utility limits under all scenarios (peak, off-peak, seasonal) and with acceptable voltage unbalance and quality. Current/thermal constraints cap conductor and transformer loading at (and often below) their continuous/emergency ampacity, accounting for ambient temperature and duty cycle. Losses are typically bounded or minimized to control I^2R energy and costs.

Service voltage windows follow ANSI C84.1 Range A ($0.95 <= |V| <= 1.05$ p.u.) and EN 50160 (~ ±10% for 95% of the week) as reference; unless stated, we enforce 0.95–1.05 p.u. with sensitivity to 0.90–1.10 p.u. for stress testing.

A scientifically defensible way to limit the number of simultaneous EVs per bus is to treat it as a hosting-capacity problem bounded by service-voltage compliance and equipment ampacity: bus voltages must remain within the utility window (e.g., ANSI C84.1 Range A ≈ 0.95–1.05 p.u.; EN 50160 ~±10% for 95% of the week), and line/transformer currents must stay below thermal ratings under realistic coincidence of charging [19]–[23]. In typical LV contexts served by common residential/service transformers (often 25–50–100 kVA), multiple Level-2 chargers can quickly dominate the local load; utility and research studies show that even three concurrent EVs can set a new nightly peak and materially erode thermal headroom and transformer life on smaller units. On 25-kVA cases, NREL's transformer-thermal work observed accelerated aging as the number of 6.6-kW vehicles increased; utility guidance similarly notes that three EVs starting together may create a new peak on a residential transformer. Given these voltage and thermal constraints and the location-specific nature of hosting capacity a planning cap of ≤3 EVs per bus is a conservative, standards-aligned assumption unless a local time-series study demonstrates higher feasible concurrency without breaching voltage limits or ampacity.

Vehicle-to-Grid (V2G) is the bidirectional use of EVs as flexible grid resources: when prices or grid needs rise, parked EVs discharge power back to the grid; when they fall, they charge. Through a bidirectional charger and an aggregator, fleets can provide peak shaving, frequency regulation, spinning reserves, and local voltage/VAR support often without disrupting drivers if state-of-charge (SoC) and departure times are honored.

Constraints and limits

- SoC bounds and departure targets: $SoC_{min} <= SoC_{(t)} <= SoC_{max}$.
- Voltage limit trigger $0.95 <|V|$.

In this study, photovoltaic (PV) farms are treated as time-varying injections of active power at specified nodes in the distribution network. the daily $PV_{(t)}$ profile at quarter-hour/hour resolution into a time-series power flow to assess its impact on terminal voltages, I^2R losses, and line/transformer loading. This keeps the model close to operational reality: solar output varies over the day and directly affects current flows and voltage margins.

Practically, PV farm effects are most apparent around midday and late afternoon; at high penetration, local voltages can rise and reverse power flow toward the substation may occur, while currents on sections near the injection points decrease and losses fall when injection is collocated with loads. Therefore, using PV as a planning lever to reduce feeder losses and support voltage while keeping an eye on permissible voltage limits and equipment loading. When combined with EV charging, PV typically does not reduce the residential evening peak, but it is highly valuable with daytime loads (workplaces/fleets) or when storage or modest curtailment is available to ensure compliance with constraints.

In our scenarios, varying both the penetration level and the spatial placement: a single large plant versus distributing injections across multiple nodes near load pockets. We then evaluate the same performance indicators compliance with voltage windows, currents and equipment loading, and losses and infer the feeder's hosting capacity with PV present. This brief introduction frames PV farms in a way that directly serves our analysis without delving into panel structural design or tracking systems.

In our setup, grid-connected PV farms are modeled as time-varying injections of active power at selected distribution nodes, with no energy storage. Practically, PV behaves as a daytime "negative load": it reduces local currents and I^2R losses when sited near demand but cannot shift energy into the evening, so it does not mitigate the residential evening peak or late-day EV charging unless those loads occur during daylight (e.g., workplaces or fleets).

Operationally, we feed the quarter-hour/hour PV(t) profile into time-series power flow and enforce our standard constraints: service-voltage windows, line/transformer ampacity, and acceptable losses. With no batteries, sunrise/sunset ramps matter: the transition from negative to positive net load must be compatible with power source.

PV generation curve shows how a solar plant's output changes over a day see fig.5, it's near zero at night, ramps up after sunrise, peaks around solar noon, then ramps down to zero by sunset a smooth "bell" shape.

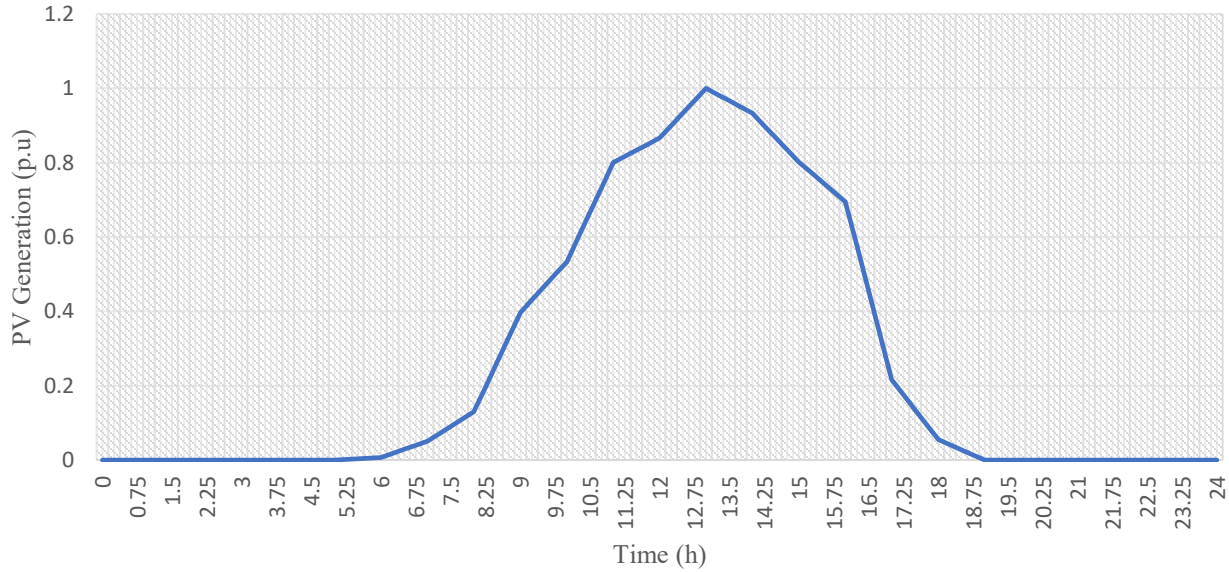

Fig. 5: PV Generation Curve.

In this setup, grid-connected wind farms are modeled as time-varying injections of active power at selected distribution nodes, with reactive power handled by a fixed power factor or basic Volt/Var support from the turbine converters. We feed the quarter-hour (or hourly) $P_{wind(t)}$ profile into time-series power flow and assess its impact on service-voltage compliance, I^2Rlosses, and line/transformer loading, the same evaluation pipeline used for other resources.

Compared with PV, wind output is less regular and can ramp faster, because it follows wind speed (and its diurnal/seasonal patterns). In many locations wind is stronger at night or in cooler seasons, so it may complement daytime PV but still cannot "shift" energy on its own, there's no storage in this study.

Wind energy generation curve that shown in Fig. 6 in our study is simply the time-series of wind-farm output injected at selected distribution nodes. Unlike PV's smooth midday bell, wind is irregular: calm periods push power down, gusts ramp it up, and short plateaus can appear when winds hover near rated speed. Treating this curve as a time-varying negative load at 15-minute/hourly resolution and feed it into time-series power flow to check the same constraints that used elsewhere, service-voltage limits, and losses. Practically also see the conceptual framework in Fig. 7 [30]-[31].

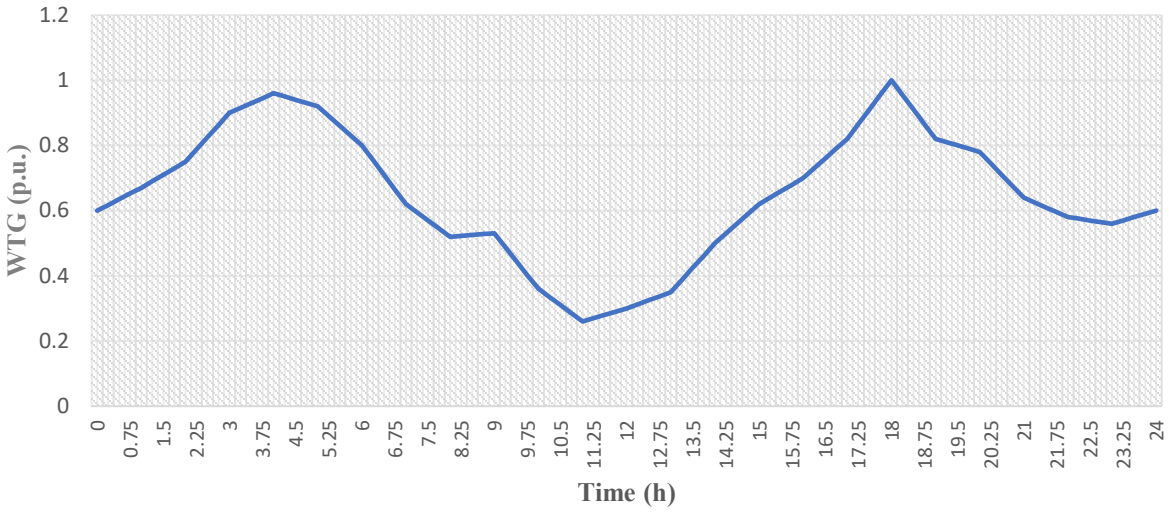

Fig. 6: Wind Energy Generation Curve.

In the analysis, PV and wind resources are represented as time-varying injections of active power at selected distribution nodes, Quarter-hour or hourly profiles PV(t) and Pwind(t) are fed into time-series power flow, and standard constraints are enforced: service-voltage windows, line/transformer ampacity, and acceptable losses. When voltages approach upper limits, modest curtailment is applied; no dedicated storage is assumed for PV or wind.

Vehicle-to-Grid (V2G) is included as a bidirectional EV resource that can discharge to the grid during constrained periods and charge during low-demand hours. Aggregated EV fleets are scheduled subject to state-of-charge and departure-time constraints so that evening peaks can be shaved and local voltage support can be provided without violating equipment limits. V2G injections and absorptions are treated like other nodal injections in the power-flow, while adhering to utility interconnection and inverter settings respecting any limits set for battery cycling. The conceptual framework of the current method is outlined in Fig 7.

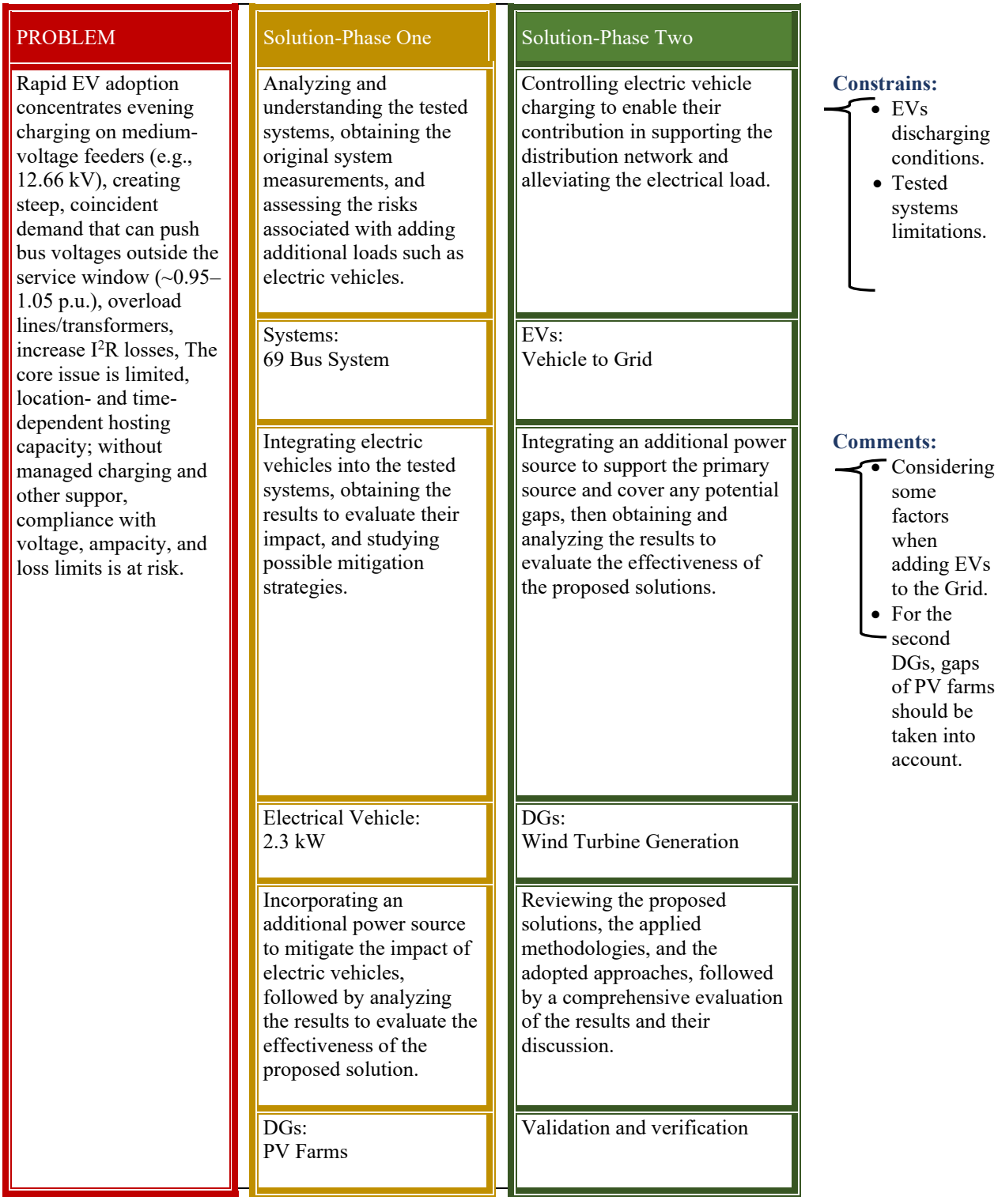

Fig. 7: Conceptual Framework.

3. RESULTS

This section presents and interprets the simulation results for the proposed EV-Charging/V2G and DG integration schemes on the IEEE test feeders. The section is structured around key performance indicators source current I_{src} minimum nodal voltage Vmin and its location, and total real power losses (TPL) and contrasts their evolution across the day under different scenarios (baseline load, PV at selected buses, WTG, and the combined PV+WTG with EV/V2G). We first decompose the net source power using the daily load curve and component traces (PV, WTG, EV charging and discharging) to highlight how generation and fleet behaviour shift the feeder demand over time. Network quality is then assessed via voltage and line-current box plots and a voltage heatmap, which together reveal spatial as well as temporal trends and periods when the 0.95 p.u. threshold is approached. To link these patterns to operational stress, report source-current trajectories and a 3-D map of branch losses and annotate the global minima and maxima of I_{src} and TPL with their timestamps. Finally, examine fleet dynamics through "Charging vs. Waiting" counts and SOC trajectories both aggregated (selected buses) and individual (tracked EVs) to explain how V2G triggers and DG availability modulate evening peaks and midday relief. Throughout, tables summarize the extrema (values, buses, and times), while the discussion emphasizes the mechanisms behind improvements or degradations e.g., midday PV loss reduction versus evening charging–induced voltage dips and the partial mitigation provided by V2G.

3.1. Base System

A common reference against which all enhanced scenarios are evaluated is established in this subsection. The base system is defined as the IEEE radial feeder operating under its native load only without electric-vehicle (EV) charging, without vehicle-to-grid (V2G) dispatch, and without distributed generation. Power-flow was solved over a 24-hour horizon with 15-minute resolution using the backward/forward sweep algorithm applied to a single-phase equivalent, so that the intrinsic loading pattern and electrical behaviour of the feeder (losses, voltage depressions, and branch currents) are captured without external interventions.

As Fig. 8, Fig. 9 and table 1 show the run reports total real losses ≈ 225.1 kW, source current 223.6 A, and a minimum voltage of 0.909 p.u. at Bus 65. With the customary 69-bus planning limit of ≈357 A per link, the source is comfortably below its current limit (≈37% headroom). The loss level corresponds to roughly 6% of feeder real load, which is consistent with a long radial feeder serving predominantly lagging PF demand.

The profile exhibits a modest sag from the substation to the mid-feeder, then a step near Bus 28 (a lateral that is electrically closer to the source), after which voltages hover near unity up to Bus 50. A steep decline from Buses 57–65 culminates in the worst node at Bus 65 (0.909 p.u.), violating the operating band 0.95–1.05 p.u. (though still within the 0.90–1.10 sensitivity band). The subsequent jump on the 66–69 lateral is expected, those branches are fed from upstream buses 11 and 12, so they see shorter electrical distance and higher voltages than the deep tail around 61–65. The cluster of sizable loads around Bus 61 (and nearby nodes 64–65) is the main driver of the local voltage depression.

The gradual sag from the substation toward the mid-feeder is a cumulative R/X effect downstream load causes higher current in upstream segments, increasing I·Z drops. The local step change around Bus 28 is associated with a discrete change in feeder conditions at that point (e.g., a lateral/branch junction and or a concentrated load block that increases downstream current).

Losses are dominated by upstream I^2R feeding the 59–65 corridor; that same corridor is your binding voltage constraint even before EV uptake. Adding EV demand there will likely push the minimum below 0.90 p.u. at peaks and increase losses; by contrast, placing EV chargers on electrically stronger buses (e.g., near the substation trunk, or on the 28–51 lateral) is far less intrusive unless paired with local DG support.

Use this baseline to report, per 15-min interval, (i) daily real losses, (ii) minimum voltage with bus and timestamp, (iii) count/share of buses violating 0.95–1.05 p.u., and (iv) any branch-current exceedances versus the 357 A planning limit.

Then drive ESM + PSO to minimize losses and voltage deviation under those constraints, with decision variables covering EVs, DG siting/sizes, and PV-WTG/V2G set-points. Expect that localized DG will raise the minimum above 0.95 p.u. and reduce losses versus baseline, while relocating or time-shifting EV demand prevents creating a new bottleneck.

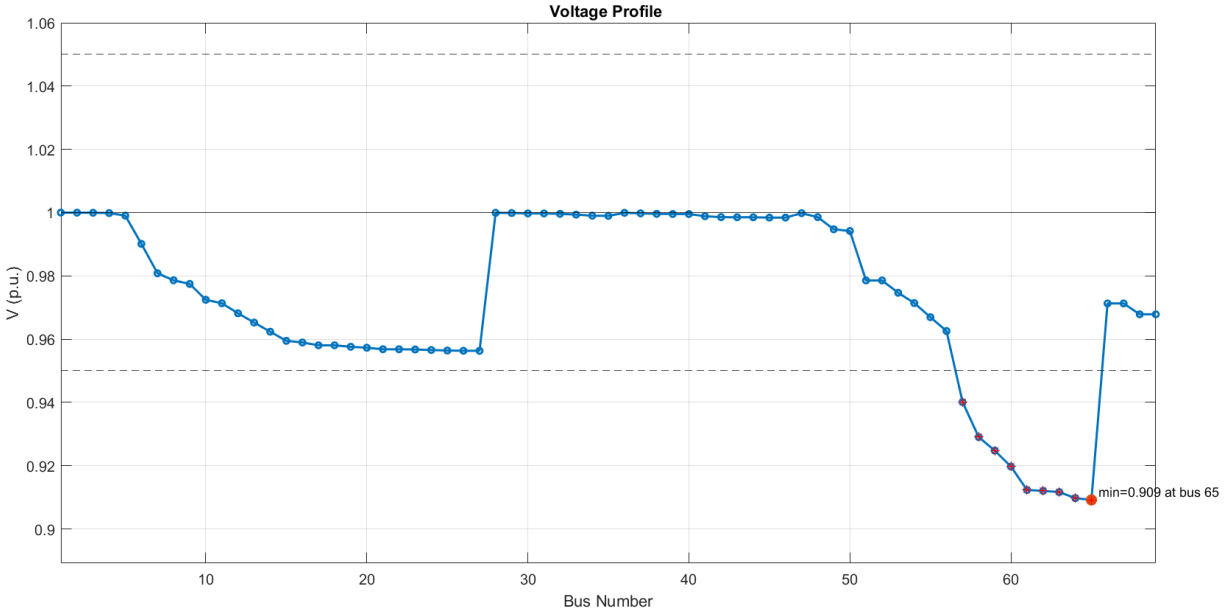

Fig. 8: Voltage Profile of Base 69-Bus System.

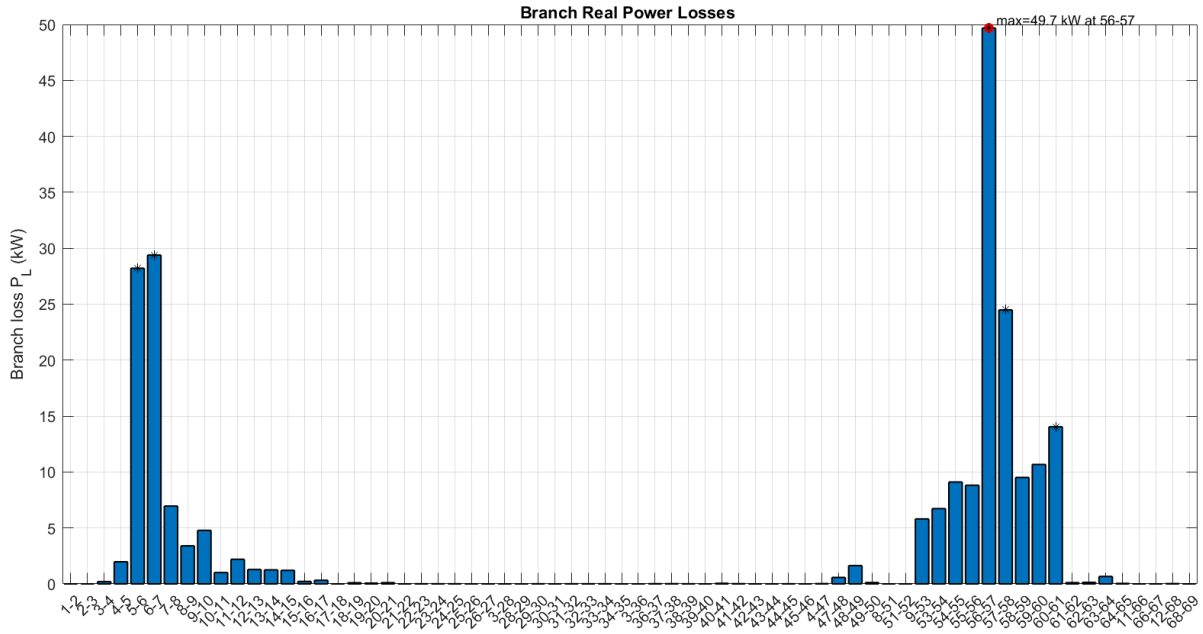

Fig. 9: Power Loss of Base 69-Bus System.

Table 1. 69-Bus Base Daily System Extremes Values.

I_{src}	223.63 A		
V_{min}	0.9092	**At Bus**	65
TPL	225.11 kW	**Time**	All the day

3.2. Grid to Vehicle-69 Bus System

Even with 69 bus system during 24 h of 15-min steps, EV arrivals are concentrated in the evening. This creates a clear peak around 18:30 h, where the source current as Fig. 10 and Fig. 11 show rises from a quiet-period level of 232.7 A at 0.00 h to 291.6 A at 18.50 h. The system real-power losses track that rise: TPL increases from 409.0 kW (0.00 h) to 543.5 kW (18.50 h), an increment of roughly +33% relative to the off-peak value. After the arrival wave subsides, both current and losses begin to decline.

The voltage box-plots in Fig. 12 and Fig. 13 show systematic depression along downstream buses, with the lowest values at the tail of the feeder. The heatmap confirms a widespread crossing of the 0.95 p.u. contour after ~18 h. The worst-bus voltage reaches 0.825 p.u. at Bus 65 (18.50 h), indicating a severe deviation (≈ −17.5% from nominal) and clear non-compliance with common ±10% operating limits. The timing aligns with the evening charging peak, so the under-voltage is primarily driven by coincident EV demand rather than baseline load alone.

Line-current distributions are highest on the trunk segments near the substation (Lines 1–3) and on a secondary cluster around the mid-feeder (≈ Lines 52–57), which feed large downstream blocks. The source current plateaus near 290 A during the peak window, consistent with the elevated branch currents. While these values appear below typical thermal limits for the 69-bus benchmark, the margin is noticeably reduced at the peak and will shrink further under higher EV penetration.

The TPL time series and the 3-D surface of branch losses in Fig. 14 and Fig. 15 show that the evening peak is not only higher in magnitude but also more spatially concentrated: losses swell on long, high-impedance sections supplying the far end of the feeder. Because losses scale roughly with I^2R, even modest reductions in peak current through coordination or localized support translate directly into meaningful loss savings.

Further insight is provided by Fig. 13, which presents a voltage heatmap across all buses over the simulated day. The heatmap makes it clear how voltage variations are distributed both spatially (along the feeder) and temporally (across time steps). The lowest-voltage regions occur during high-demand periods, and they predominantly appear at downstream buses where the accumulated line impedance and increased current lead to larger voltage drops. This visualization complements the single time-slice voltage profiles by revealing when and where undervoltage risk is most likely to occur.

Fig. 14 complements the voltage heatmap by showing the corresponding distribution of branch real-power losses. Losses are concentrated on the upstream branches that carry the aggregated feeder current, while branches feeding heavily loaded laterals exhibit secondary peaks. The loss surface also highlights the strong coupling between EV-driven load peaks and loss magnification (since losses scale approximately with the square of branch current). Together, Figs. 13–14 provide a clearer interpretation of how time-varying EV charging impacts both voltage compliance and feeder efficiency, and they motivate the later scenarios in which local PV/V2G support is used to reduce current flow and mitigate losses.

The “Charging vs. Waiting” plot in Fig. 16 and Fig.17 indicate that the system hits capacity in the 18–22 h window: up to ~160–165 EVs charging concurrently, with a waiting queue of ~40–45 EVs. Average SOC on the sampled buses rises steadily through the evening; individual traces at Bus 7 show vehicles reaching near-full SOC before midnight. In other words, the grid is not energy-constrained across the day, but power-constrained during a short, highly coincident interval.

Under uncoordinated G2V behavior as in table 2, the 69 feeder exhibits strong evening coincident demand that drives under-voltage at the extremities and ~33% higher real-power losses at peak relative to off-peak. Adding modest reactive/voltage support offer the largest impact-per-cost.

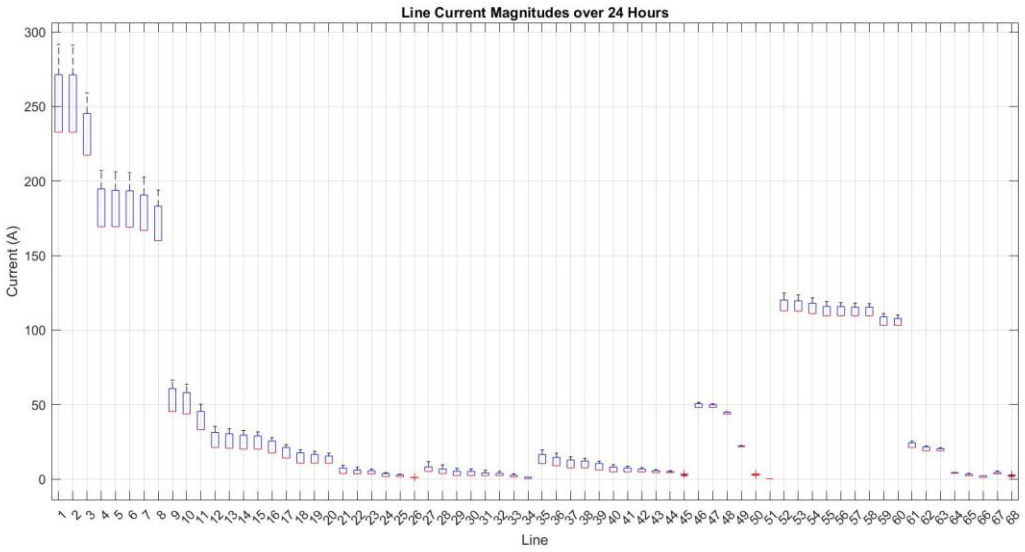

Fig. 10: Line Current of G2V 69-Bus System.

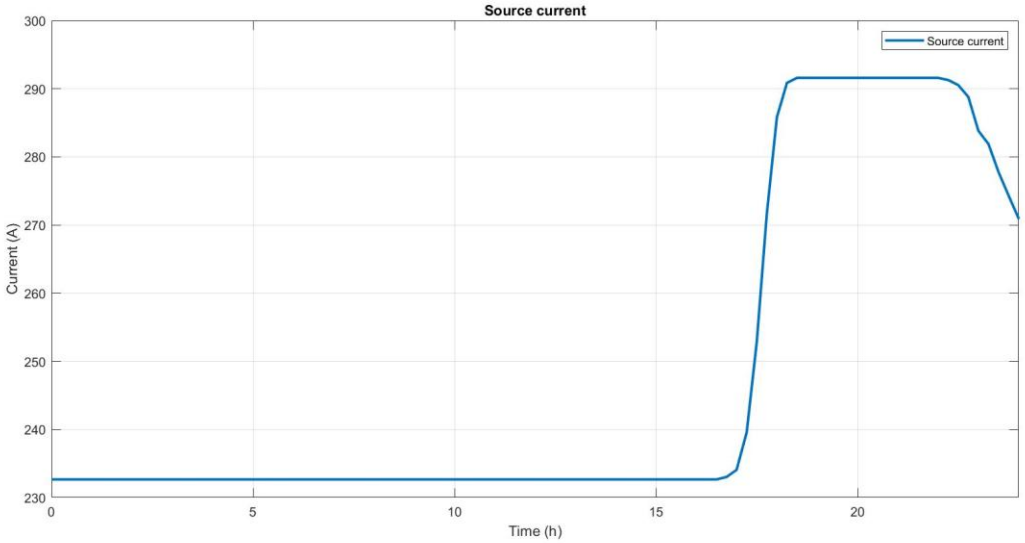

Fig. 11: Source Current of G2V 69-Bus System.

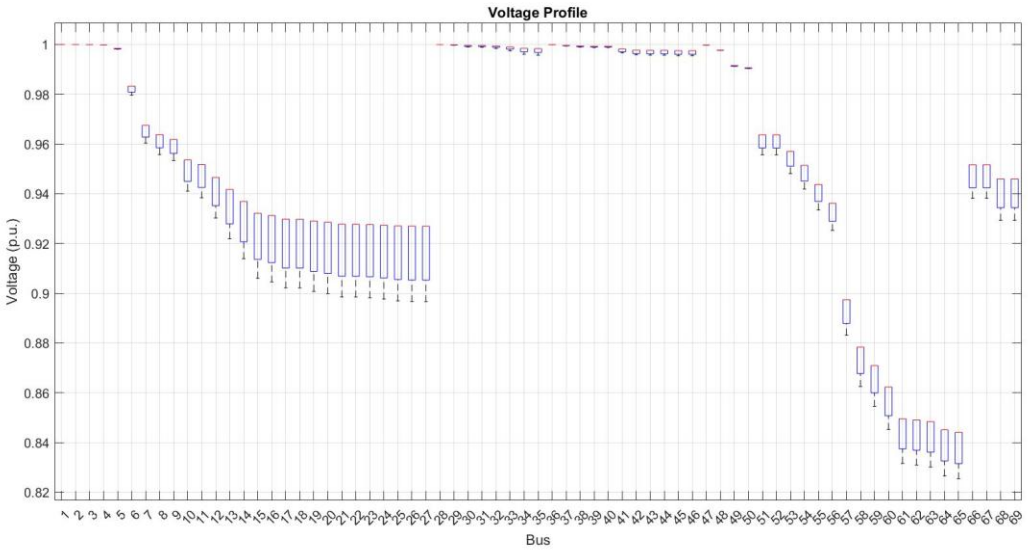

Fig. 12: Voltage Profile of G2V 69-Bus System.

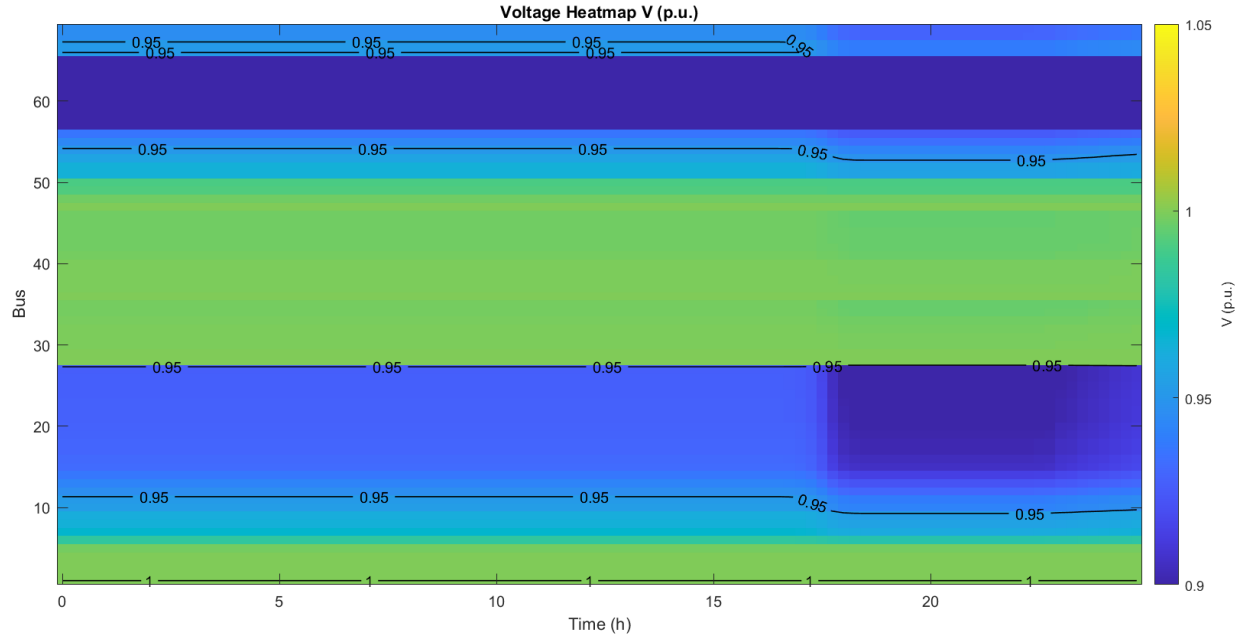

Fig. 13: Voltage Heatmap of G2V 69-Bus System.

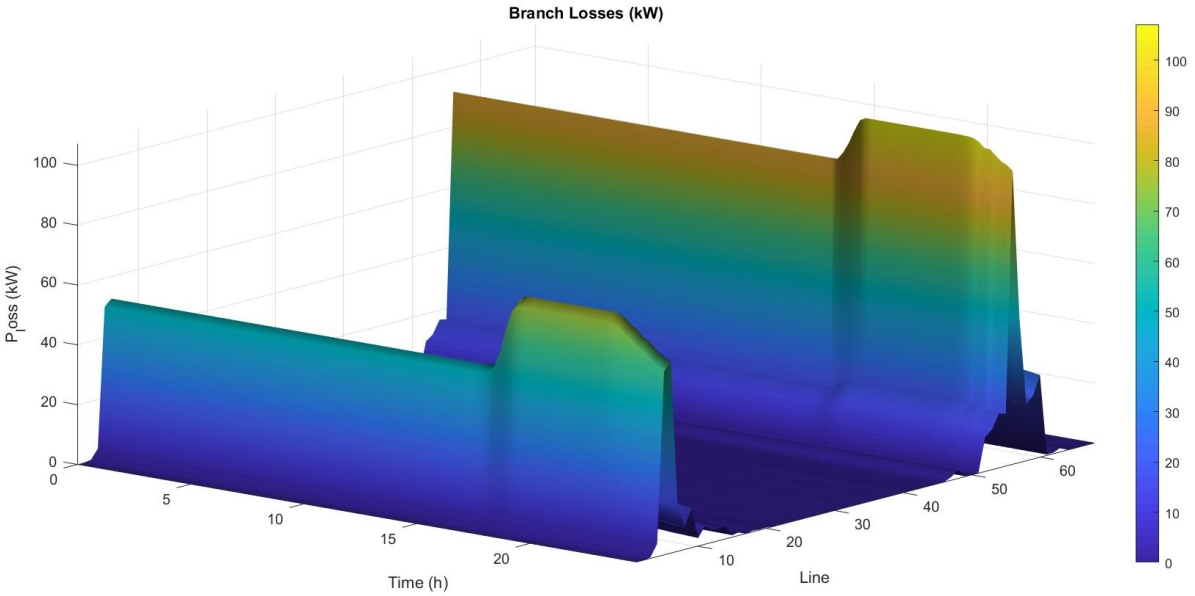

Fig. 14: Branch Loss of G2V 69-Bus System.

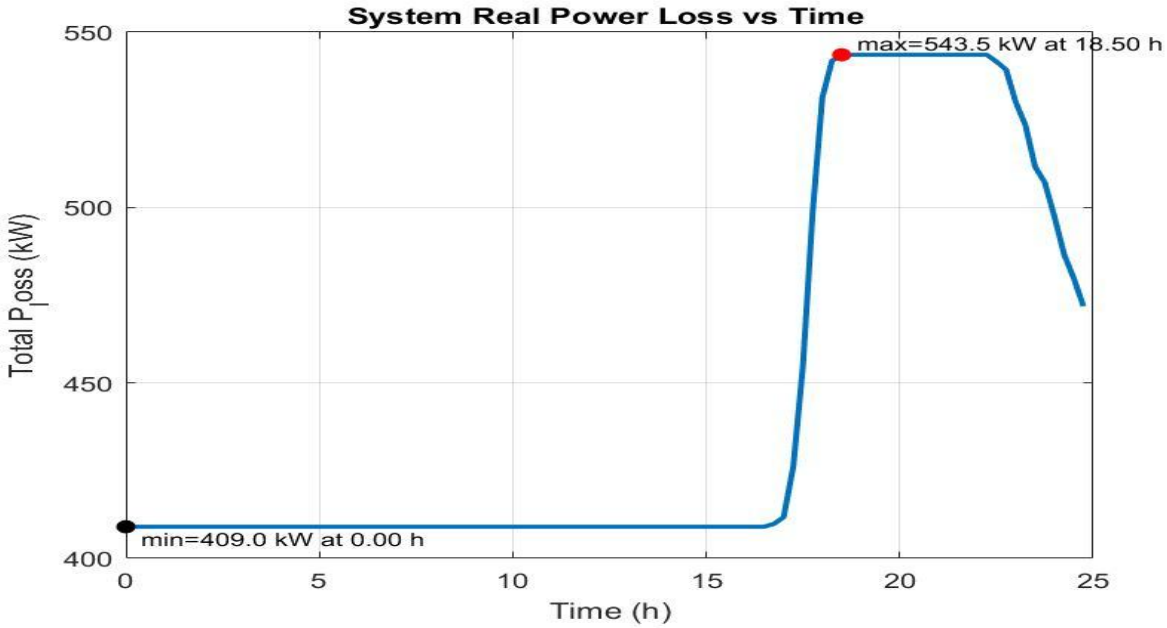

Fig. 15: System Real Loss of G2V 69-Bus System.

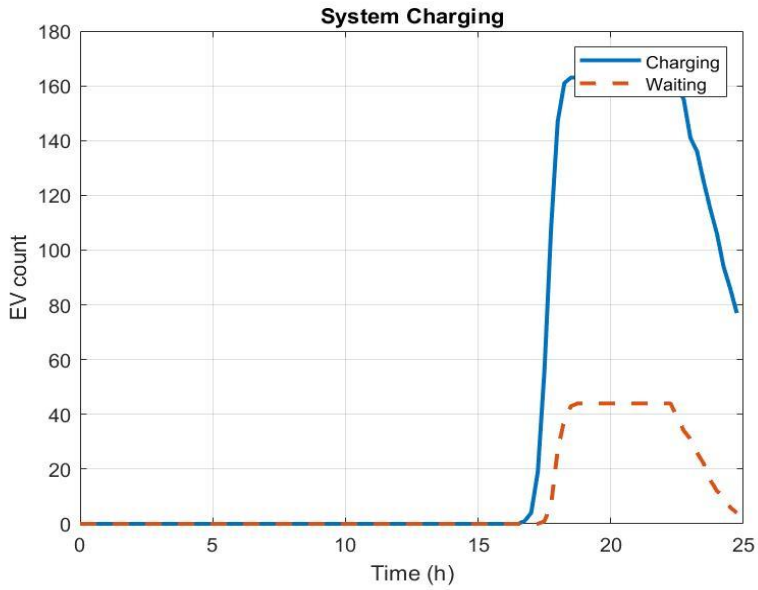

Fig. 16: Charging of G2V 69-Bus System.

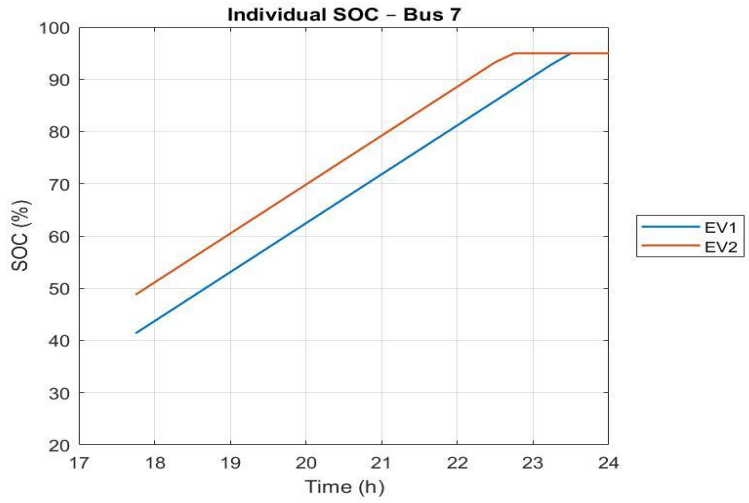

Fig. 17: Individual SoC of G2V 69-Bus System.

Table 2. 69-Bus G2V Daily System Extremes Values.

$\mathbf{I_{src,min}}$	232.7 A			**Time**	0.00 h
$\mathbf{I_{src,max}}$	291.6 A			**Time**	18.50 h
$\mathbf{V_{min}}$	0.825	**At Bus**	65	**Time**	18.50 h
$\mathbf{TPL_{min}}$	409.0 kW			**Time**	0.00 h
$\mathbf{TPL_{max}}$	543.5 kW			**Time**	18.50 h

3.3. PV/Vehicle to Grid

In this subsection, the joint impact of photovoltaic distributed generation (PV-DG) and vehicle-to-grid (V2G) operation on the radial test feeder is assessed under the same demand and arrival patterns used previously. PV output is applied via

a time-varying irradiance profile and fixed power factor, while V2G is enabled by a voltage-triggered policy: when the local voltage drops below 0.95 pu, eligible EVs (with SOC ≥ 70%) are discharged toward a lower bound of 50% SOC; recharging toward a 95% target is resumed once system conditions allow. Power-flow calculations are performed with the backward/forward-sweep method using per-phase injections for all sources and loads.

The combined PV/V2G case is analyzed in terms of feeder voltages, branch currents, source current, and total power losses over the 24-hour horizon. Attention is given to the evening peak, during which V2G support is expected to raise the minimum bus voltage, reduce trunk current plateaus, and curtail loss growth relative to the EV-only case. Midday intervals are examined for possible reverse-power flow and for shifts in reactive-power exchange caused by the prescribed PV and V2G power factors. Charging-queue dynamics and SOC trajectories are included to quantify how much flexibility is delivered by the connected fleet.

Overall, the PV resource is expected to offload daytime demand and shape the daily net-load curve, while V2G provides targeted support during low-voltage periods. The presented plots (time series, box-plots, and heat maps) are used to quantify these effects and to highlight any trade-offs such as increased branch loadings on specific segments or reactive-power burdens thereby informing voltage-security and hosting-capacity considerations for the feeder.

Loss Sensitivity Factor – 69 Bus System

To identify a candidate location for a single DG unit, a loss sensitivity factor (LSF) pre-screen is used, in which the highest value indicates that bus sensitive for a small change in active power (defined here as $\Delta P = 0.01$ pu on the system base), so the results of applying LSF and indicates that bus number 61 is the best location of implementing DG shown in Fig. 18.

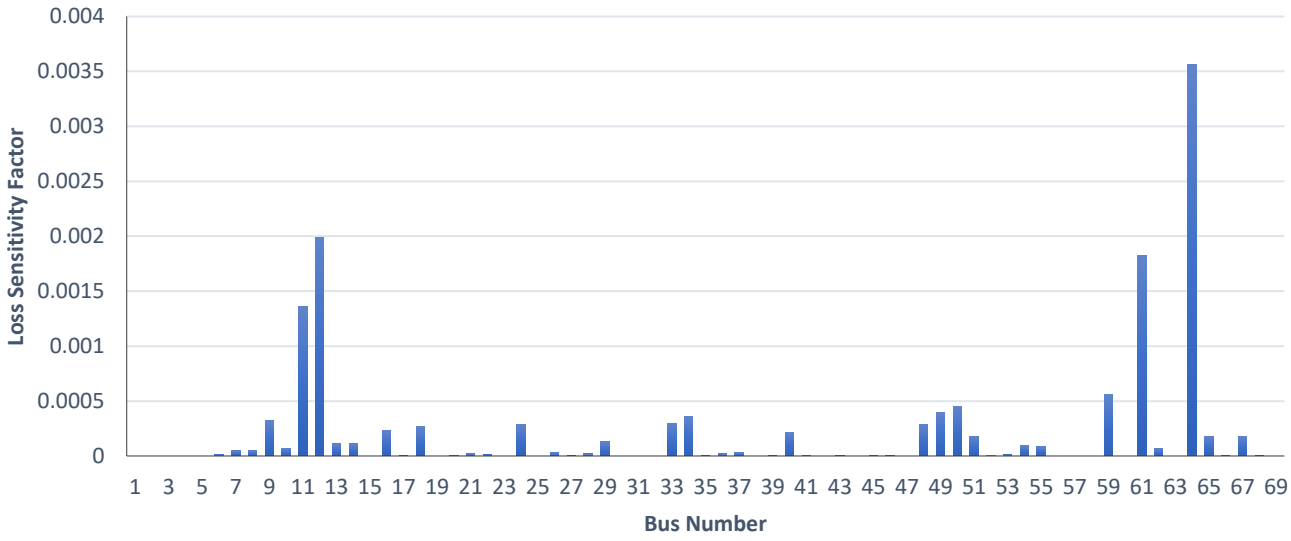

Fig. 18: Loss sensitivity factor for 69-Bus system.

This subsection evaluates 24-hour simulation of the 69-radial feeder with stochastic EV arrivals, V2G support that is activated whenever a local bus drops below 0.95 p.u., and a PV plant connected at Bus 61 (≈1.82 MW, pf≈0.81 lagging). The PV profile peaks at midday while EV charging is concentrated in the early evening. All results are per-phase, solved with a forward/backward-sweep load flow.

The net power in Fig. 19 seen by the substation follows the expected pattern: PV production pushes the source power and current down through the middle of the day and the evening EV wave drives them back up. Quantitatively, the minimum source current as shown in Fig. 20 and Fig. 21 occurs around the PV peak, ≈ 113 A at 13.00 h, while the maximum arrives

during the EV surge, ≈ 280 A at 19.00 h. The Daily Load Curve also shows several-hundred-kilowatt V2G discharge emerging during 18–22 h; this visibly trims the peak but does not fully offset the charging demand once PV output collapses after sunset.

Voltage behavior in Fig. 22 and Fig. 23 reflects the same diurnal split. Midday, PV at Bus 61 lifts voltages along the downstream tail (Buses ~61–66), pulling the 0.95 p.u. contour upstream and reducing dispersion in the box plots. After sunset, support disappears and the weakest section collapses under the EV wave. The worst voltage is $V_{min} \approx 0.899$ p.u. at Bus 65 around 19.00 h, coincident with the source-current maximum. This is a clear violation of the 0.95 p.u. planning threshold despite V2G assistance, indicating that evening remains the binding constraint for voltage quality.

Line-current statistics show the thermal picture. The highest magnitudes appear on the trunk segments near the substation and on a secondary cluster of laterals that feed large downstream blocks. Variability increases markedly during 18–22 h, aligning with EV arrivals and the source-current plateau. While currents remain below typical benchmark ampacities in this run, safety margin narrows at the peak and would erode quickly with higher EV penetration.

Losses that shown in Fig. 24 and Fig. 25 follow the familiar I^2R pattern. With PV production high, feeder currents and total real-power loss drop to a minimum of ≈ 23.2 kW at 13.00 h. During the evening charge window, currents rise across many branches and losses grow accordingly to a maximum of ≈ 295.1 kW at 19.00 h. The 3-D branch-loss surface confirms that losses concentrate on the upstream backbone and on heavily loaded laterals; PV reduces both the magnitude and spatial spread of losses around noon.

Queueing and SOC traces in Fig. 26 and Fig. 27 illustrate how the control behaves at the vehicle level. Charging is negligible until ~17 h, then ramps sharply; waiting queues peak in the same window as the source and loss maxima. Individual-vehicle SOC trajectories at a sample bus show the intended policy: vehicles charge toward ~70 %, discharge down toward ~50 % when V2G is triggered by a local undervoltage event, and resume charging once conditions relax. This behavior delivers grid support exactly when and where voltages are weakest, but the aggregate V2G power in this setup is not yet large enough to prevent the late-evening voltage violation.

Overall, PV sited deep in the feeder (Bus 61) strongly reduces midday loading as table 3 shows, currents, and losses and improves the local voltage profile. The evening remains critical, with V_{min} =0.899 p.u. at Bus 65 and $I_{src,max} \approx 280$ A despite V2G. Practical remedies include increasing V2G participation or discharge caps specifically for 18–22 h, adding reactive support near the 61–66 tail (capacitor/regulator), modest reconductoring of the weakest spans, or relocating/duplicating PV closer to the most constrained nodes. Without such measures, especially under higher EV adoption one should expect deeper voltage dips, higher branch-current peaks, and disproportionate growth in I^2R losses during the evening hours.

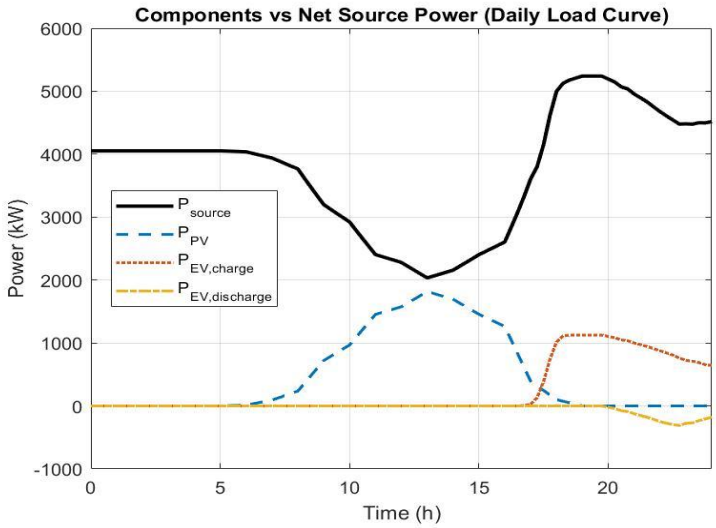

Fig. 19: Daily Load Curve of PV/V2G 69-Bus System.

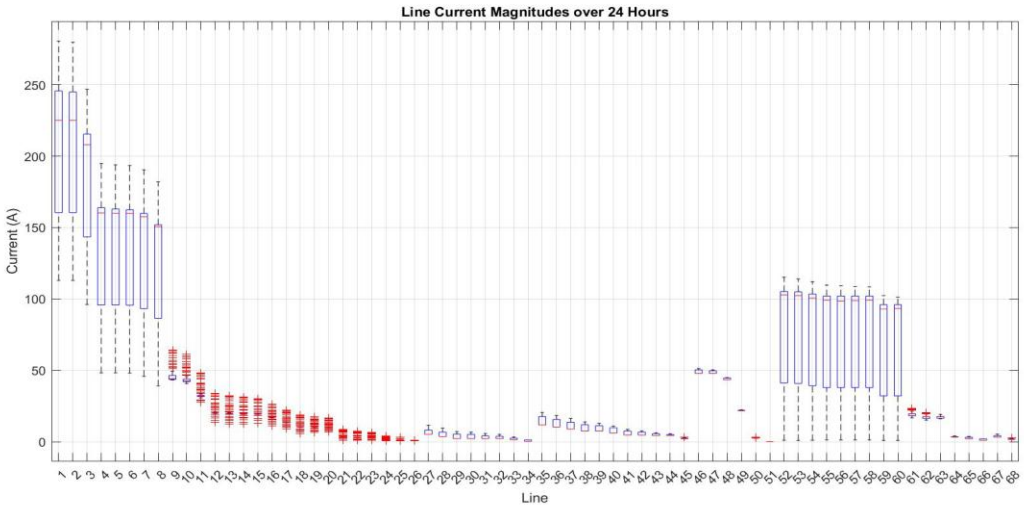

Fig. 20: Line Current of PV/V2G 69-Bus System.

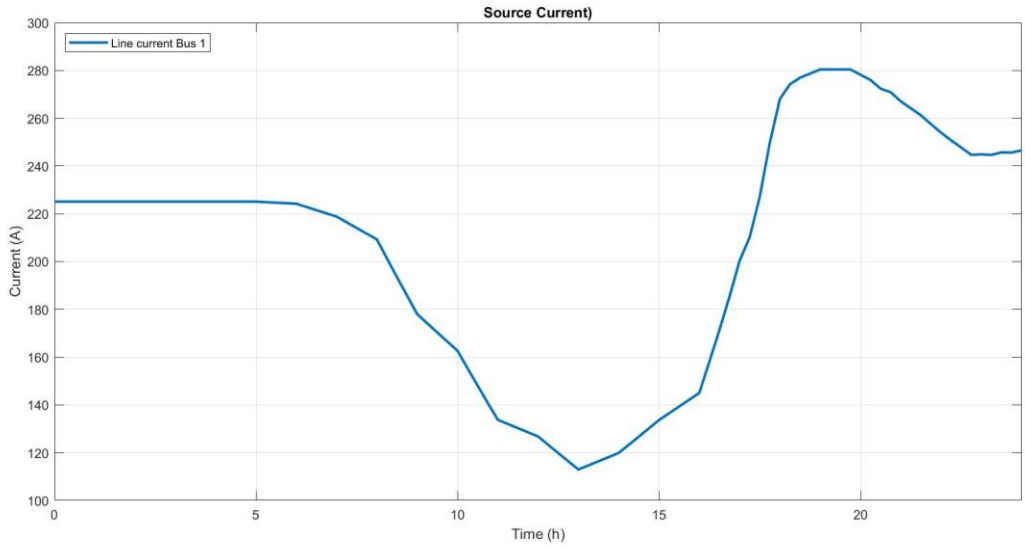

Fig. 21: Source Current of PV/V2G 69-Bus System.

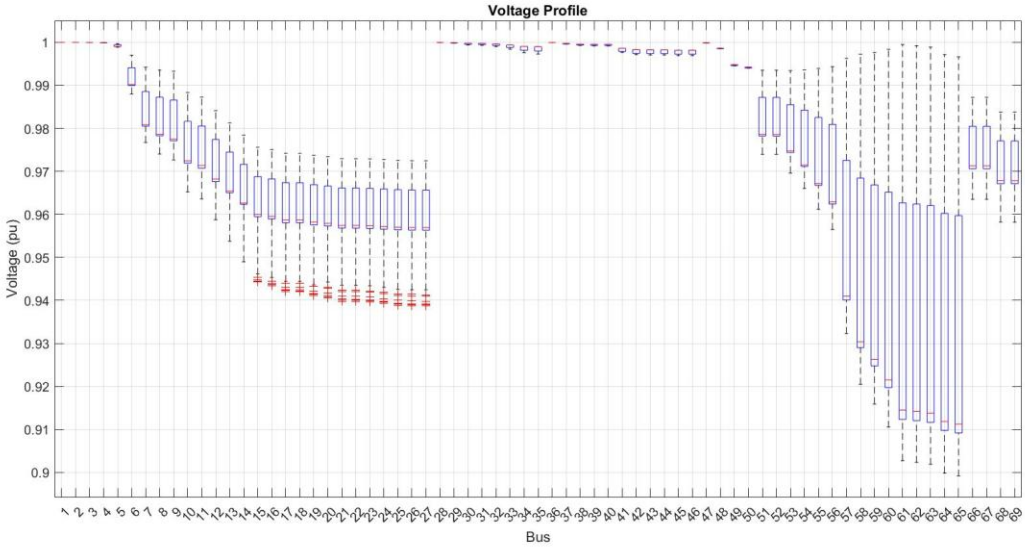

Fig. 22: Voltage Profile of PV/V2G 69-Bus System.

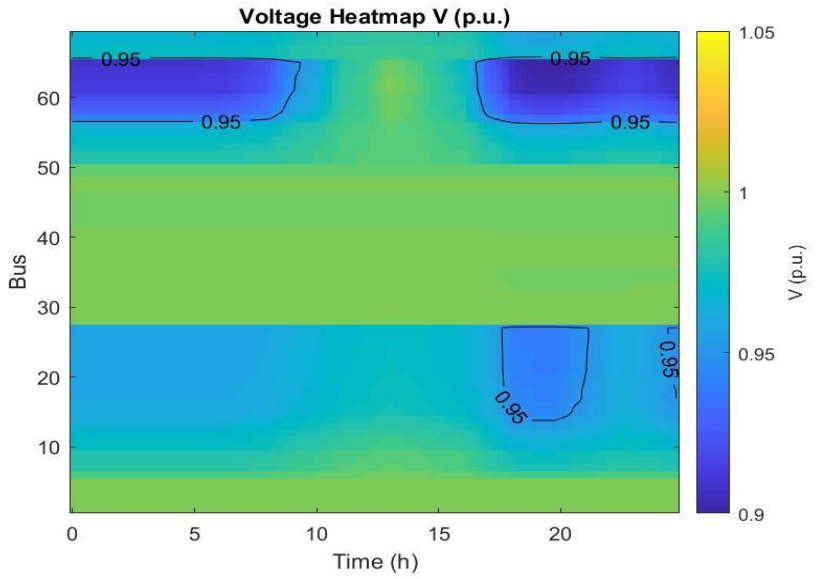

Fig. 23: Voltage Heatmap of PV/V2G 69-Bus System.

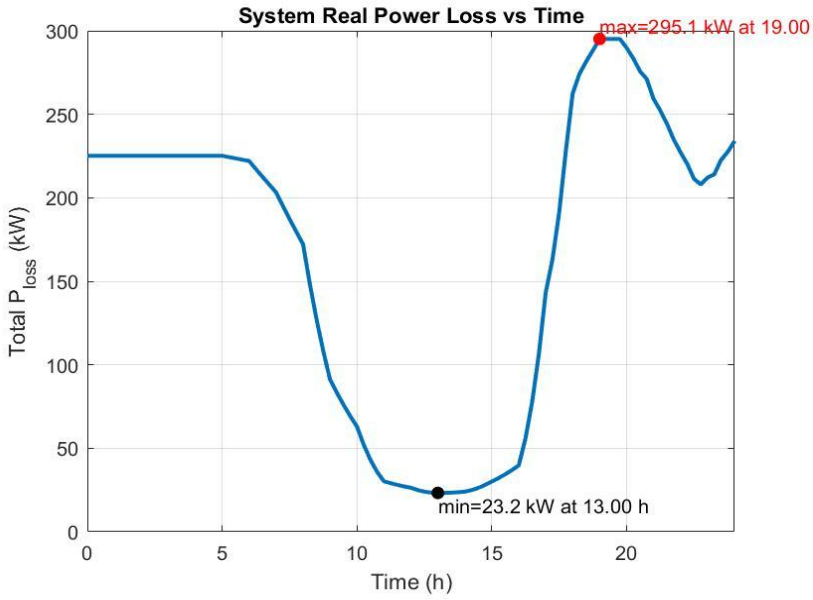

Fig. 24: System Real Loss of PV/V2G 69-Bus System.

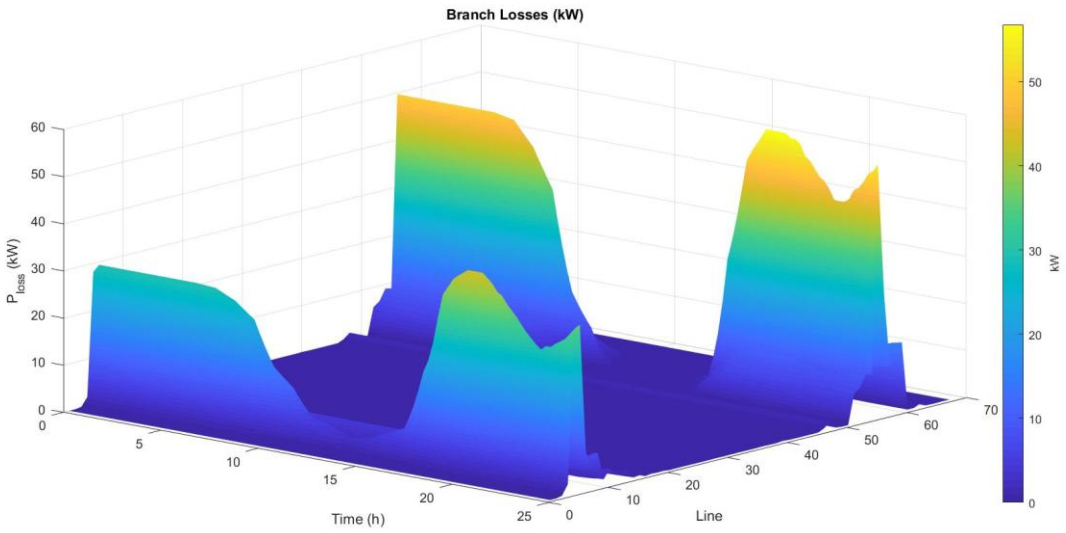

Fig. 25: Branch Loss of PV/V2G 69-Bus System.

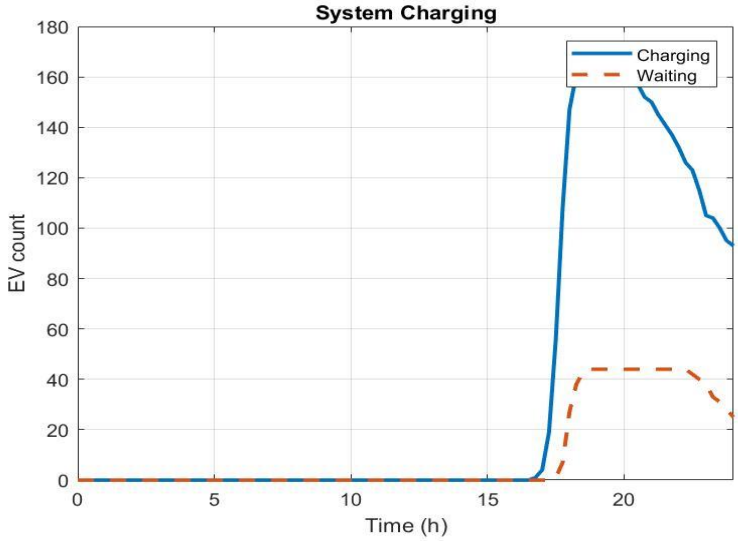

Fig. 26: Charging of PV/V2G 69-Bus System.

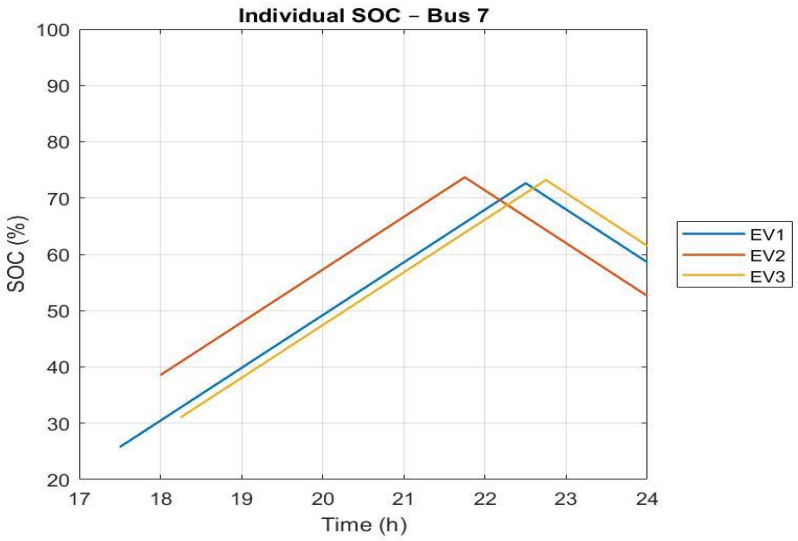

Fig. 27: Individual SoC of PV/V2G 69-Bus System.

Table 3. 69-Bus PV/V2G Daily System Extremes Values.

$\mathbf{I_{src,min}}$	113.0 A			**Time**	13.00 h
$\mathbf{I_{src,max}}$	280.4 A			**Time**	19.00 h
$\mathbf{V_{min}}$	0.899	**At Bus**	65	**Time**	19.00 h
$\mathbf{TPL_{min}}$	23.2 kW			**Time**	13.00 h
$\mathbf{TPL_{max}}$	295.1 kW			**Time**	19.00 h

3.4. PV-WTG/Vehicle to Grid

In this subsection, the joint impact of distributed photovoltaic (PV) and wind turbine generation (WTG) in the presence of Vehicle-to-Grid (V2G) operation is assessed over a 24-hour horizon with 15-minute resolution. Time-varying active-power profiles were applied to both PV and WTG, each enforced at a fixed lagging power factor, while V2G was activated by a voltage trigger: when any local bus dropped below 0.95 pu, eligible EVs (SOC ≥ 70%) were discharged down to SOC = 50%, after which normal charging toward 95% SOC resumed. Three-phase injections and loads were modeled per phase, and network states were computed via backward/forward sweep power-flow.

The daily net-power plot shows that PV at Bus 17 and the wind unit at Bus 61 flatten the midday demand seen by the substation, while the evening EV influx drives the peak. PV ramps up from early morning, peaks around noon, and fades after ~16:00; the wind generator contributes across most hours with a broad shoulder. As a result, the source power reaches its lowest band in late afternoon when DG support is still present and before EV arrivals and then climbs to its highest level in the evening once PV has vanished and EV charging dominates. EV discharging remains modest, which indicates that the V2G voltage trigger is seldom met while EVs are connected.

The source current in Fig. 28 and Fig. 29 follows the same story. It is lowest during the DG-supported afternoon and highest during the evening charging window. Quantitatively, the simulation gives a minimum of 122.4 A at 04:00, when the base load is light and no EVs are present, and a maximum of 205.9 A at 22:00, coincident with the largest charging cohort. This alignment between current and net source power confirms that DG primarily reduces upstream transfers in daylight hours, while EV charging shifts the feeder's stress to the evening.

Voltage statistics across buses reveal a typical radial pattern: voltages are close to 1.0 p.u. near the source and decline toward the tail see Fig. 30 and Fig. 31. The worst case occurs at the far end of the network with V_{min} = 0.936 p.u. at Bus 65 around 11:00. Importantly, this minimum appears before the evening EV arrivals; therefore, V2G cannot mitigate this

midday depression, and the wind unit at Bus 61, although helpful later does not fully arrest the drop at the extreme end during peak PV export and mid-feeder flow reversals.

Line-current boxplots highlight heavier utilization in the upstream sections (Lines 1–6) that carry the bulk of transfers, while mid-feeder segments experience lower currents. Distinct clusters are visible around the laterals tied to DG locations, reflecting periods of bidirectional flow. Evening outliers on selected downstream lines coincide with the EV charging surge, consistent with increased local loading and higher feeder diversity.

Fleet and individual EV behavior match the arrival profile in Fig. 32 and Fig. 33: charging ramps sharply after ~17:00, a modest waiting queue forms at the peak, then both decline as vehicles complete their sessions. Tracked SOC at Bus 64 typically climbs into the 70–75 % band before tapering. Small SOC reductions late in the evening point to brief local V2G discharges when the voltage dips, but these events are infrequent and do not materially change the feeder-level evening peak.

System losses substantiate the flow patterns. The total real-power loss reaches a daytime minimum of 23.7 kW at 16:30 when PV+wind support suppresses upstream transfers, and a daytime maximum of 105.6 kW at 11:00, which coincides with the worst far-end voltage at Bus 65 see Fig. 34 and Fig. 35. The 3-D branch-loss surface shows localized “hot spots” on upstream lines during the evening EV peak and on deep laterals around mid-day, capturing the temporal shift of where the feeder dissipates energy.

Overall, DG smooths the day while EVs shape the night. The midday voltage constraint is fundamentally a spatial issue at the far end that appears when EVs are scarce; therefore, two classes of mitigations are most promising: enabling volt/var support from PV and wind (absorbing or injecting reactive power as needed) and strengthening mid-feeder voltage support via strategically placed capacitors/regulators or by relocating part of the PV capacity deeper in the feeder. On the demand side, incentivizing midday workplace/public EV charging would put batteries on the grid precisely when the far-end voltage is weakest, improving both compliance and losses without raising the evening peak see table.4.

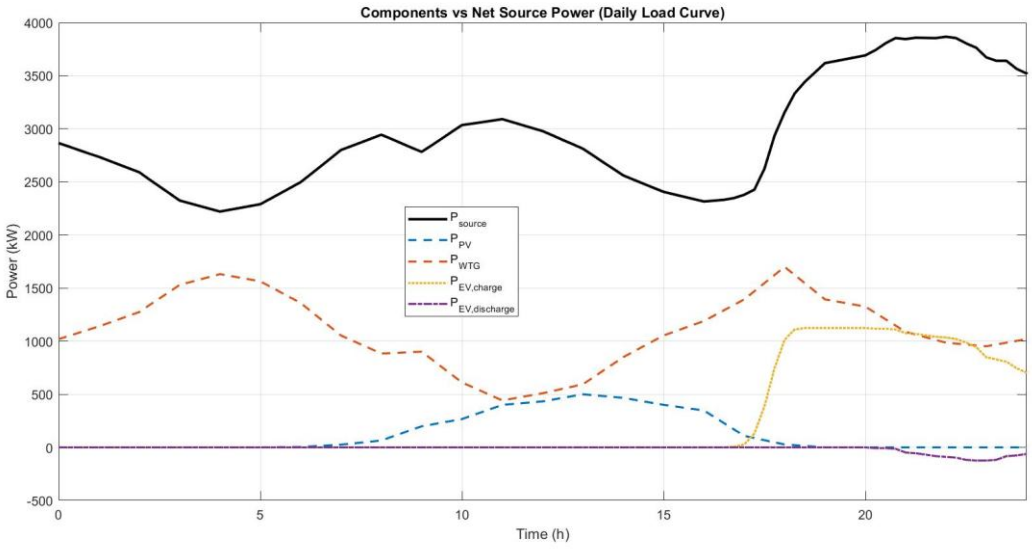

Fig. 28: Daily Load Curve of PV-WTG/V2G 69-Bus System.

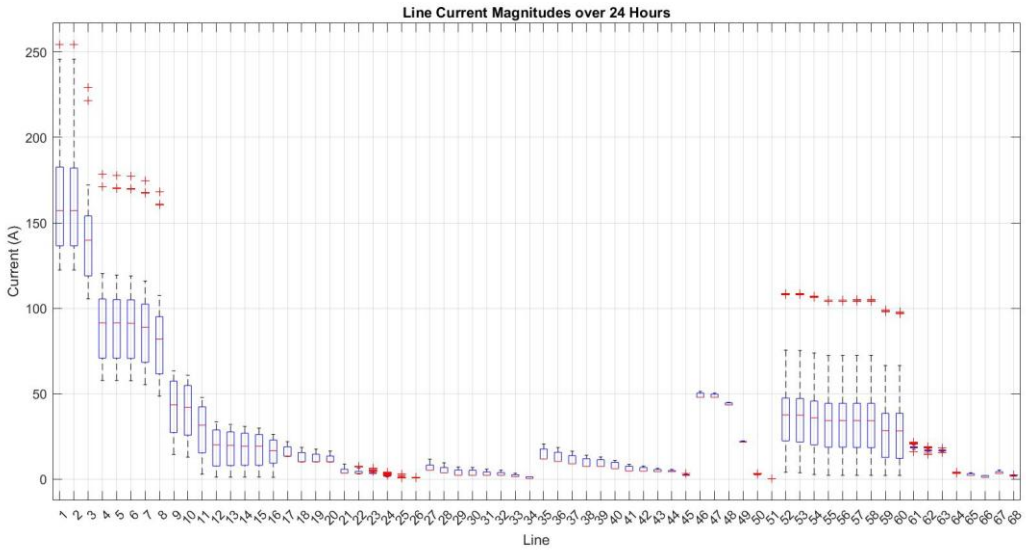

Fig. 29: Line Current of PV-WTG/V2G 69-Bus System.

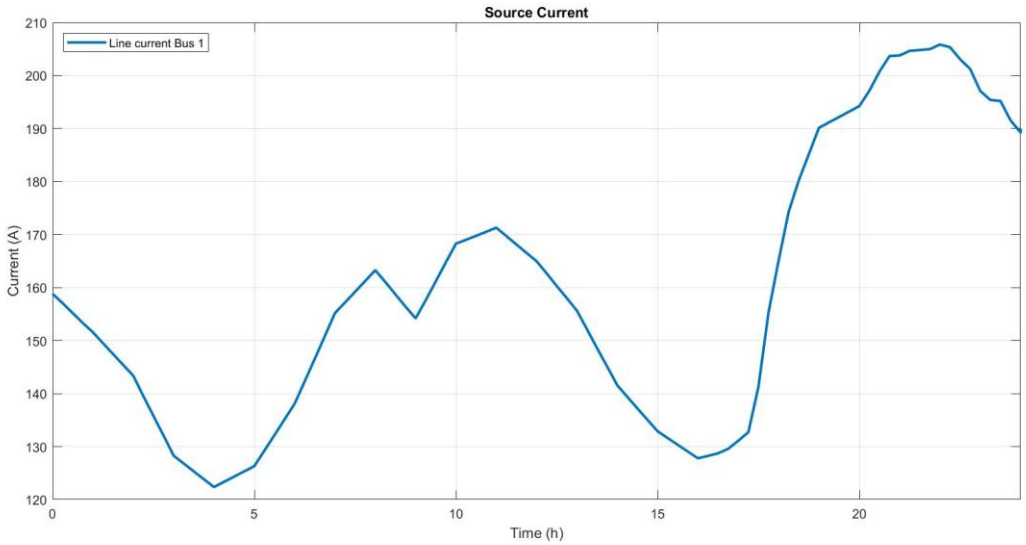

Fig. 30: Source Current of PV-WTG/V2G 69-Bus System.

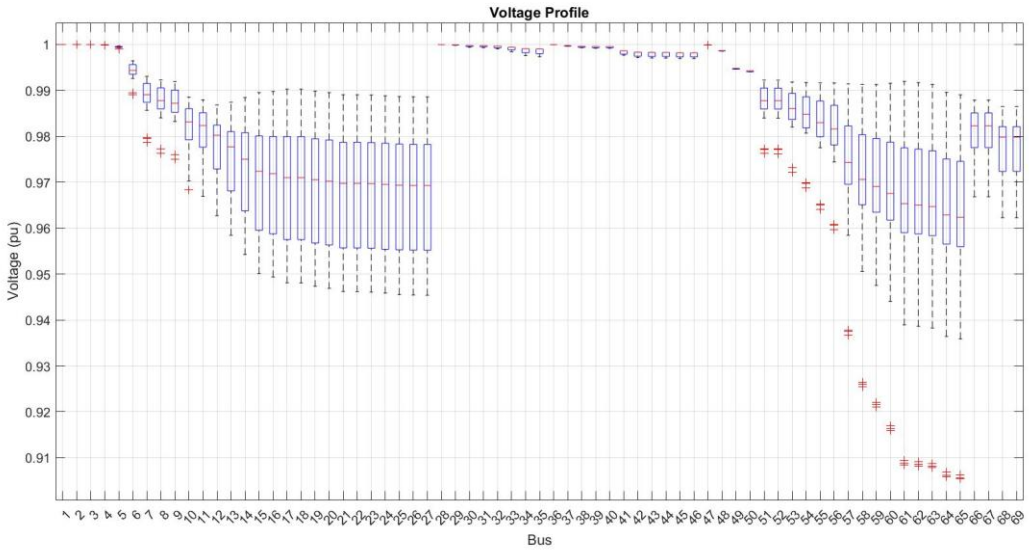

Fig. 31: Voltage Profile of PV-WTG/V2G 69-Bus System.

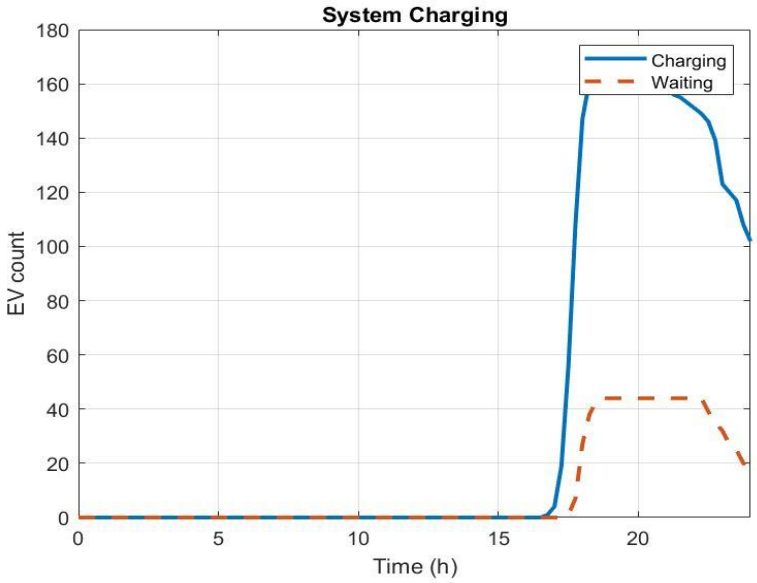

Fig. 32: Charging of PV-WTG/V2G 69-Bus System.

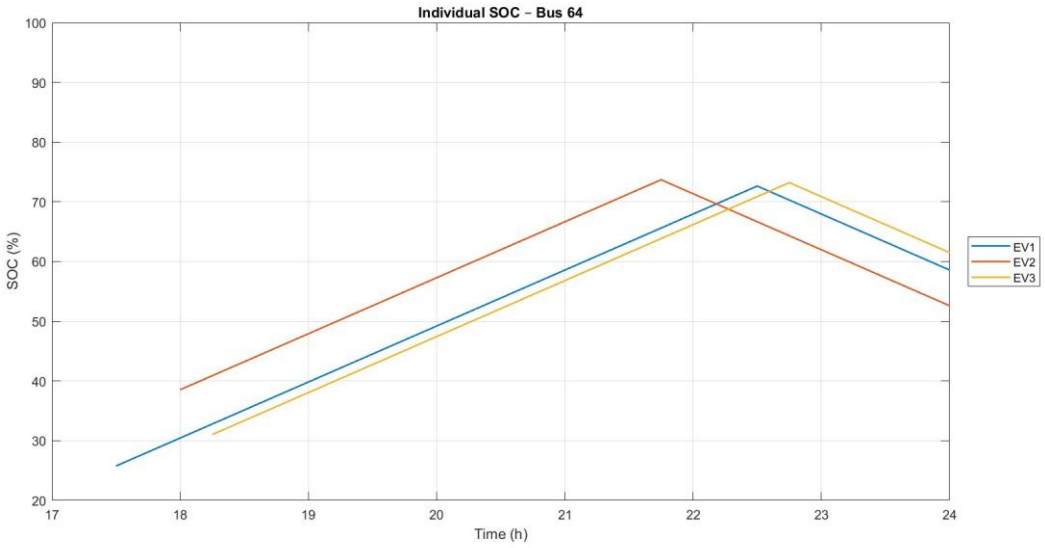

Fig. 33: Charging of PV-WTG/V2G 69-Bus System.

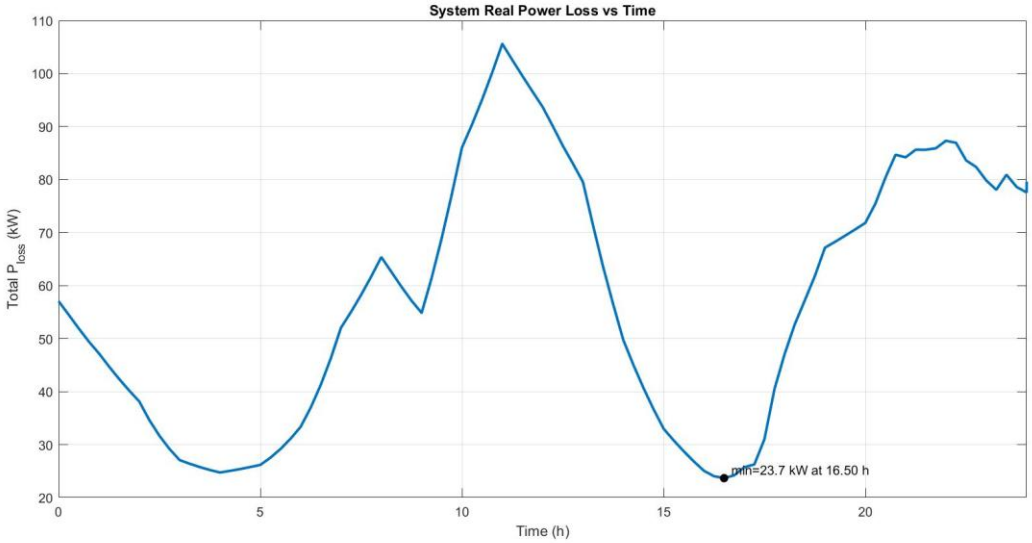

Fig. 34: System Real Loss of PV-WTG/V2G 69-Bus System.

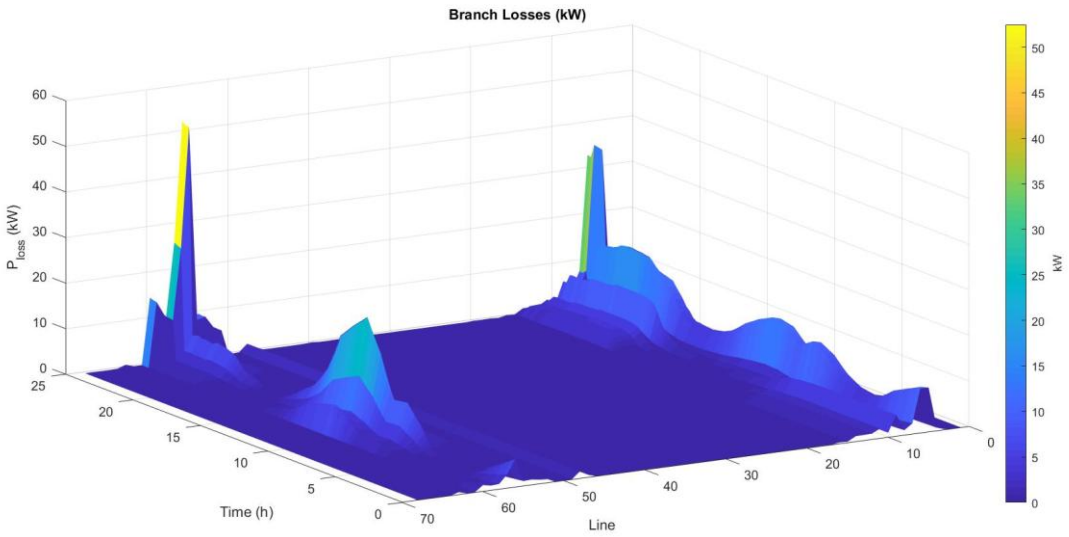

Fig. 35: Branch Loss of PV-WTG/V2G 69-Bus System.

4. CONCLUSIONS

Time-series simulations on the IEEE-69 radial feeder indicate that transport electrification is feasible without limit breaches when charging is feeder-aware and DERs are properly placed and controlled; in the baseline (no EV/PV/WTG/V2G), daily losses were ≈225.1 kW, source current ≈223.6 A, and the minimum voltage 0.909 p.u. at bus 65, whereas unmanaged evening charging (G2V) pushed source current to ≈291.6 A at 18:50, lowered the minimum voltage to 0.825 p.u. at bus 65, and raised losses to ≈543.5 kW (vs. 409.0 kW at 00:00). Adding feeder-sited PV with a pragmatic V2G trigger reduced midday transfers ($I_{src,min}$ ≈113.0 A at 13:00) and losses (≈23.2 kW at 13:00), though late-afternoon/evening intervals remained binding ($I_{src,max}$ ≈280.4 A; Vmin ≈0.899 p.u. at 19:00). Combining PV+WTG with V2G improved the full-day profile: Vmin increased to 0.936 p.u. (11:00 at bus 65), the maximum observed losses fell to ≈105.6 kW (11:00), and $I_{src,max}$ declined to ≈205.9 A (22:00). Across scenarios, unmanaged evening charging produced the sharpest excursions higher upstream currents, deeper voltage depressions, and higher I^2R losses while moderate charging coordination improved voltage compliance and thermal headroom; co-siting DER capacity near load pockets and along electrically "long" laterals localized support and reduced upstream flows; and short-duration V2G support shaved residual peaks and lifted the minimum-voltage profile without large stationary storage. Overall, feeder-aware charging, conservative inverter droops (Volt/Var, Volt/Watt), and selective reinforcements raised hosting capacity while maintaining comfortable voltage margins and containing losses. The novelty of this work lies in providing a unified, time-series (15-min) assessment of EV charging (G2V), V2G support, and distributed PV/WTG integration on a benchmark radial distribution feeder under consistent voltage/thermal constraints. The main contributions are: (i) an integrated modeling and simulation framework (BFS-based) that couples feeder power-flow constraints with EV/V2G and DER operating profiles, (ii) a systematic scenario comparison that quantifies trade-offs between upstream current, minimum-voltage compliance, and I^2R losses across the day, and (iii) practical, design-oriented insights on how feeder-aware charging and localized DER/V2G support can increase hosting capacity and reduce peak stress without relying on large stationary storage.

REFERENCES

[1] S. Rahman, I. A. Khan, A. A. Khan, A. Mallik, and M. F. Nadeem, "Comprehensive review & impact analysis of integrating projected electric vehicle charging load to the existing low voltage distribution system," Renewable and Sustainable Energy Reviews, vol. 153, p. 111756, Jan. 2022, doi: 10.1016/j.rser.2021.111756.

[2] A. Tayri, M. Remaoun, H. Hadj Abdallah, and M. Denaï, "Grid Impacts of Electric Vehicle Charging: A Review," Energies, vol. 18, no. 14, p. 3807, 2025, doi: 10.3390/en18143807.

[3] M. O. Khan, S. Iqbal, and M. R. Islam, "Impact assessment of electric vehicle charging on distribution networks," IET Generation, Transmission & Distribution, 2024. (Online early). doi: 10.1049/gtd2.

[4] I. Chandra, S. Maheshwari, and S. Singh, "A comprehensive review on coordinated charging of electric vehicles: methods, energy management, and ancillary services," Sustainable Cities and Society, 2024. (Online early). doi: 10.1016/j.scs.2024.

[5] M. Al-Dhaifallah, M. A. Al-Hasan, and M. AlShamrani, "Enhancing hosting capacity for electric vehicles in modern distribution networks," Scientific Reports, vol. 14, 2024, Art. no. 76410, doi: 10.1038/s41598-024-76410-0.

[6] O. A. Balogun, A. N. Hasan, and A. R. Al-Ajlan, "Coordination of smart inverter-enabled distributed energy resources for voltage regulation: A review," Sustainable Energy, Grids and Networks, vol. 38, 2024, Art. no. 101222, doi: 10.1016/j.segan.2024.101222.

[7] S. M. S. Ullah, M. A. H. Mondol, and T. K. Roy, "Techno-economic impacts of Volt-VAR control on the high PV penetration network considering IEEE 1547-2018," Sustainable Energy, Grids and Networks, vol. 33, 2023, Art. no. 100069, doi: 10.1016/j.segan.2023.100069.

[8] N. A. Brohi, M. A. Sorgdrager, and D. L. Maskell, "Advances in Hosting Capacity Assessment and Enhancement for Distribution Networks: A Review with Focus on Dynamic Operating Envelopes," Energies, vol. 18, no. 11, p. 2922, 2025, doi: 10.3390/en18112922.

[9] G. Lankeshwara, P. R. A. S. Ariyaratne, and M. Nadarajah, "A review on network-aware control of distributed energy resources: dynamic operating envelopes," Renewable and Sustainable Energy Reviews, 2025. (Online early). doi: 10.1016/j.rser.2025.

[10] Y. Zhuang, Y. Wang, and J. Zhao, "Real-time hosting capacity assessment for electric vehicles: probabilistic forecasting and risk analysis," Applied Energy, 2025. (Online early). doi: 10.1016/j.apenergy.2025.

[11] S. S. Barhagh, M. Shafie-khah, J. P. S. Catalão, and P. Siano, "Optimal sizing and siting of electric vehicle charging stations under uncertainty," IEEE Transactions on Intelligent Transportation Systems, vol. 25, no. 6, pp. 5668–5682, 2024, doi: 10.1109/TITS.2023.3334470.

[12] S. Ray, M. B. Hossain, and M. R. Islam, "Review of electric vehicles integration impacts in distribution networks," Sustainable Cities and Society, vol. 102, 2023, Art. no. 104946, doi: 10.1016/j.scs.2023.104946.

[13] D. Hua, F. Peng, S. Liu, Q. Lin, J. Fan, and Q. Li, "Coordinated Volt/Var Control in Distribution Networks Considering Demand Response via Safe Deep Reinforcement Learning," Energies, vol. 18, no. 2, p. 333, 2025, doi: 10.3390/en18020333.

[14] Z. Wu, H. Zhang, and Y. Liu, "Distributed voltage control for multi-feeder distribution networks using robust deep reinforcement learning," Applied Energy, 2025. (Online early). doi: 10.1016/j.apenergy.2025.XXXXXX.

[15] C. Liddell, R. K. Bell, and J. R. Manser, "Telematics-Based Managed EV Charging: A Pilot Case Study," SAE Technical Paper 2025-01-8122, 2025, doi: 10.4271/2025-01-8122.

[16] K. Łowczowski, P. M. Skowroński, and A. R. Michalski, "Analysis of the Impact of Volt/VAR Control on Harmonics and Resonance in Distribution Networks," Energies, vol. 17, no. 22, p. 5561, 2024, doi: 10.3390/en17225561.

[17] S. Petridis, et al., "An Efficient Backward/Forward Sweep Algorithm for Power Flow Analysis through a Novel Tree-Like Structure for Unbalanced Distribution Networks," Energies, vol. 14, no. 4, 2021. DOI: 10.3390/en14040897

[18] E. Bompard, R. Napoli, and F. Xue, "Convergence of the backward/forward sweep method for power flow solutions in distribution networks," Int. J. Electr. Power Energy Syst., vol. 22, no. 3, pp. 163–167, 2000. DOI: 10.1016/S0142-0615(00)00009-0

[19] M. Milovanović, et al., “A backward/forward sweep power flow method for distribution systems with nonlinear loads,” Engineering Reports, 2020. DOI: 10.1002/2050-7038.12310
[20] R. C. Dugan and T. E. McDermott, “An Open Source Platform for Distribution System Simulation,” Proc. IEEE PES General Meeting, 2011. DOI: 10.1109/PES.2011.6039829
[21] R. C. Dugan and T. E. McDermott, “Distribution System Analysis and the OpenDSS,” Proc. IEEE PES Transmission & Distribution Conf. and Exposition, 2012.
[22] R. C. Dugan, “OpenDSS Application Examples for Smart Distribution Systems,” Proc. IEEE PES General Meeting, 2013.
[23] R. D. Zimmerman, C. E. Murillo-Sánchez, and R. J. Thomas, “MATPOWER: Steady-State Operations, Planning, and Analysis Tools for Power Systems Research and Education,” IEEE Trans. Power Syst., vol. 26, no. 1, pp. 12–19, 2011. DOI: 10.1109/TPWRS.2010.2051168
[24] A. Thurner, et al., “pandapower—An Open-Source Python Tool for Convenient Modeling, Analysis, and Optimization of Electric Power Systems,” IEEE Trans. Power Syst., vol. 33, no. 6, pp. 6510–6521, 2018. DOI: 10.1109/TPWRS.2018.2829021
[25] N. Cho, et al., “Evaluations on the Harmonic Allocation Methods of IEC 61000-3-6 and IEEE 519,” Electric Power Systems Research, vol. 232, 2024. DOI: 10.1016/j.epsr.2024.110260
[26] M. E. Baran and F. F. Wu, “Network reconfiguration in distribution systems for loss reduction,” IEEE Trans. Power Del., vol. 4, no. 2, pp. 1401–1407, 1989. DOI: 10.1109/61.25627
[27] T. Jayabarathi, et al., “Enhancement of distribution system performance with DERs …,” Heliyon, 2024.
[28] D. Shirmohammadi, et al., “A Compensation-Based Power Flow Method for Weakly Meshed Distribution and Transmission Networks,” IEEE Trans. Power Syst., vol. 3, no. 2, pp. 753–762, 1988. DOI: 10.1109/59.192932
[29] IEEE Distribution Planning Working Group, “Radial Distribution Test Feeders,” IEEE Trans. Power Syst., vol. 6, no. 3, pp. 975–985, 1991.
[30] H. Yang, Z. Liu, and Y. Ma, “Positive-sum game-based capacity configuration planning of solar–wind–battery for black-start,” Int. Trans. Electr. Energy Syst., Article ID 6176839, 2023.
[31] A. Eid and M. Abdel-Salam, “Management of EV charging stations in LV networks integrated with wind turbine–BESS using metaheuristics,” Engineering Optimization, online Sep. 20, 2023.

تقييم أثر دمج المركبات الكهربائية ومصادر الطاقة المتجددة على أداء نظام التوزيع

الملخص: يشكّل التزايد السريع في تبنّي المركبات الكهربائية (EV) ضغوطًا جديدة على مغذّيات التوزيع، بينما لا تزال الأدلة الكمية حول الكيفية التي يمكن بها للتوليد المتجدد المُنسَّق وتشغيل المركبة-إلى-الشبكة (V2G) التخفيف من هذه التأثيرات محدودة، خاصةً في الشبكات الشعاعية ذات الفروع الطويلة والطلب ذي الذروة المسائية. في هذه الدراسة، أُجريت محاكاة تدفّق قدرة زمنية عالية الدقة (كل 15 دقيقة) على نظام شعاعي معياري مكوَّن من 69 حافلة لتقييم الشحن غير المُدار للمركبات الكهربائية، والشحن المُدار مع محفزاتV2G ، وسيناريوهات مشتركة مع محطات كهروضوئية (PV) وتوليد توربينات رياح (WTG) مدمجة على المغذّي. استُخدم نموذج وصول عشوائي للمركبات، وتتبع لحالة شحن البطارية(SOC) ، ونموذج مبسّط للشاحن (2.3 كيلوواط لكل طور، ومعامل قدرة ≈0.95)؛ ويتم تفعيل تفريغ V2G عندما يهبط الجهد المحلي إلى أقل من 0.95 وحدة نسبية (.p.u) ويتوقف التفريغ حين تنخفض حالة الشحن إلى حد أدنى محدّد. اتّبعت مخرجات PV/WTG ملفات يومية واقعية مع معاملات قدرة متأخرة تمثل حدود العواكس. أتاح أسلوب المسح الأمامي/الخلفي في تدفّق القدرة الحصول على جهود العقد، وتيارات الفروع، وإجمالي فواقد المغذّي على أفق 25 ساعة، ثم جرى تلخيص النتائج عبر خرائط حرارية ومخططات صندوقية ومنحنيات توازن القدرة اليومية. وتبيّن أن تنسيق V2G مع موارد PV/WTG على مستوى المغذّي يقلّل ماديًا تيار المصدر الأقصى، ويخفف التحميل الزائد على العمود الرئيسي وأجزاء منتصف المغذّي، ويخفض إجمالي فواقد القدرة الفعالة، مع رفع الجهود الدنيا نحو الحدود المقبولة خلال النوافذ المسائية الحرجة. وكانت الفوائد أقوى عندما تزامن إنتاج المتجدّدات زمنيًا مع طلب الشحن، وحين كانت الموارد الموزعة قريبة كهربائيًا من الفروع المُجهَدة؛ ومع ذلك، استمرت قيود متبقية خلال ذرى آخر الليل مع ضعف دعم المتجدّدات. وبصورة عامة، تشير النتائج إلى أن عتبات V2G البراغماتية، وقدرًا متواضعًا من المتجدّدات المتموضعة على المغذّي، مع إدارة أساسية للشحن، يمكنها تحسين سعة الاستضافة بدرجة كبيرة من دون الحاجة إلى تعزيز فوري للشبكة.

كلمات مفتاحية: المركبات الكهربائية؛ شبكات التوزيع؛ من المركبة إلى الشبكة (V2G)؛ الخلايا الكهروضوئية/الطاقة الشمسية الكهروضوئية (PV)؛ التوليد بالرياح؛ تقليل فواقد القدرة؛ تنظيم الجهد.